Space Debris: Assessing Risk and Responsibility

Andrew M. Bradley

Institute for Computational and Mathematical Engineering, Stanford University, Stanford, CA 94305

Lawrence M. Wein *

Graduate School of Business, Stanford University, Stanford, CA 94305

Abstract

We model the orbital debris environment by a set of differential equations with parameter values that capture many of the complexities of existing 3-dimensional simulation models. Ignoring collisions between fragments (as is typically done), we show that the number of fragments remains bounded for all time. We compute the probability that a spacecraft gets destroyed in a collision during its operational lifetime, and then define the sustainable risk level as the maximum of this probability over all future time. Focusing on the 900-to-1000 km altitude region, which is the most congested portion of low Earth orbit, we find that – despite the initial rise in the level of fragments – the sustainable risk $< 10^{-3}$ if there is high ($> 98\%$) compliance to the existing 25-year postmission deorbiting guideline. We quantify the damage (via the number of future destroyed operational spacecraft) generated by past and future space activities. We estimate that the 2007 FungYun 1C antisatellite weapon test represents $\approx 1\%$ of the legacy damage due to space objects having a characteristic size of ≥ 10 cm, and causes the same damage as failing to deorbit 2.6 spacecraft after their operational life. Although the political and economic issues are daunting, these damage estimates can be used to help determine one-time legacy fees and fees on future activities (including deorbit noncompliance), which can deter future debris generation, compensate operational spacecraft that are destroyed in future collisions, and partially fund research and development into space debris mitigation technologies.

Key words: orbital debris, low Earth orbit, antisatellite weapon test

* Corresponding author
Email addresses: ambrad@stanford.edu (Andrew M. Bradley), lwein@stanford.edu (Lawrence M. Wein).

1 Introduction

Orbital debris generated by 50 years of space activities poses a risk for operational spacecraft, which can collide in a catastrophic manner with either another large object (e.g., an upper stage rocket body) or with a smaller fragment generated by a previous collision or by a previous explosion of a large object (Liou & Johnson, 2008). A high-fidelity 3-dimensional simulation model of low Earth orbit (LEO, which is the region between 200 and 2000 km altitude) predicts that – even with no future launches – the growth rate of collisional debris would exceed the natural decay rate in ≈ 50 years (Liou & Johnson, 2008). Moreover, the analysis in Liou & Johnson (2008) did not account for the Chinese anti-satellite weapon (ASAT) test that destroyed the FungYun 1C spacecraft in January 2007, which created the largest man-made orbital debris cloud in history (Liou & Portman, 2007). NASA's safety guidelines recommend limiting the postmission lifetime of spacecraft or upper stages in LEO to 25 years (NASA Safety Standard 1740.14, 1995). Because this measure will not prevent a positive growth-rate of debris (Liou & Johnson, 2005), it has been suggested that the removal of large intact satellites from space is also necessary (Liou & Johnson, 2006). Although the impact of satellite removal has been assessed (Liou & Johnson, 2007), currently there are no technologies that are technically feasible and economically viable (Liou & Johnson, 2006).

Space debris represents a textbook example of environmental economics (Perman et al., 2003): space is a public good (i.e., despite the 1976 Bogota Declaration, in which 8 equatorial countries claimed sovereignty over the portion of geosynchronous Earth orbit lying above their territory (Soroos, 1982), there are no well-defined and enforceable property rights and no countries are excluded from launching satellites) and debris is a pollutant. More specifically, LEO is a renewable stock resource (much like air or water), in that debris eventually dissipates, albeit on an extremely slow time scale.

The two fundamental issues in environmental economics are to determine the target level of pollution and to decide how to achieve this target. Regarding the first issue, we use the concept of sustainability (loosely defined as the highest utility that can be maintained for all future time), which has gained some popularity in recent years as an alternative to economic efficiency (Perman et al., 2003, Ch. 4), particularly for studying resources that – like outer space – have no substitutes and are in the infancy of their exploitation. More specifically, we introduce the maximum (over all future time) lifetime risk to an operational spacecraft (i.e., $\max_{t \geq 0} r^o(t)$ in Eq. (8)) as a measure of sustainability.

Regarding the second fundamental issue, there are a number of different

instruments used in environmental economics to achieve the target pollution level: technology controls, ceilings or taxes on emissions, subsidies for pollution reduction, tradeable emissions permits, and non-compliance fees. In practice, technology controls are often used because of the difficulty of measuring emissions, pollution levels, or costs, and indeed the 25-yr postmission deorbit guideline and the end-of-life passivation of rocket bodies and spacecraft (NASA Safety Standard 1740.14, 1995) are forms of technology control.

In this paper, we develop an ordinary differential equation (ODE) model that is a mean field approximation, incorporating physical principles for collision rates (Alberty & Silbey, 1997), decay rates (Rossi et al., 1994), and orbital trajectories (King-Hele, 1964), as well as rocket body and spacecraft characteristics (Kessler, 2000) and the fragmentation models and empirical distributions developed in Johnson et al. (2001). The model elucidates the nature of the ($\geq$ 10 cm) debris dynamics over both the medium (centuries) and long (millennia) term, and allows us to assess sustainability. We also use the model to estimate the damage (in terms of the future operational spacecraft that are destroyed in collisions) associated with a present-day launch or ASAT explosion, as well as the damage due to existing space objects. These damages provide a basis for quantifying one-time country-specific legacy costs and setting fees for launches and ASAT tests, which can reduce the amount of debris generation, create a compensation fund for destroyed spacecraft, and partially fund the research and development necessary to remove large objects from space.

2 The Model

We study the collisional interactions among satellites between the altitudes 900 and 1000 km, ignoring the effects of collisions in lower or higher orbits; we refer to this [900,1000] km region of space, which is the location of nearly 60% of all predicted catastrophic collisions in LEO over the next 200 years (Liou & Johnson, 2008), as the shell of interest (SOI). Our model tracks the number of rocket bodies and three types of spacecraft over time, and the effective number of four types of fragments. The effective number weights each fragment by the fraction of time its orbit is in the SOI and the probability that it is hazardous or benign (as explained below); spacecraft and rocket bodies, which together are referred to as intacts, are assumed to have circular orbits, and hence spend all of their orbital time in the SOI.

Some intacts in LEO have a deorbit capability to facilitate a 25-yr postmission lifetime in LEO in accordance with NASA guidelines (NASA Safety Standard 1740.14, 1995): at the end of its operational lifetime, such an intact immediately maneuvers to either an orbit with a lower perigee (typically

below 600 km) from which it decays naturally from LEO within 25 years, or to a disposal orbit above 2500 km altitude (intacts operating in the SOI will typically choose the former option). By deorbit, we shall mean that the intact leaves the SOI. Consequently, we differentiate the total number of spacecraft ($S(t)$) into three types: those that have a deorbit capability ($S_d(t)$); those that do not and are still operational ($S_n^o(t)$), and those that do not have a deorbit capability and are no longer operational ($S_n(t)$). (We use the same symbol for two purposes: e.g., $S_d(t)$ is the effective number of satellites of type S_d at time t.) Future spacecraft are launched into the SOI at annual rate λ_o, and we assume that some recent spacecraft and a fraction θ_d of all future spacecraft have a postmission deorbit capability. These spacecraft deorbit at rate μ_o, where μ_o^{-1} is the average operational lifetime. The majority of existing spacecraft in LEO and a fraction $1 - \theta_d$ of future spacecraft do not have a postmission deorbit capability, and change category, from S_n^o to S_n, at rate μ_o, and then deorbit naturally at rate μ_n. Similarly, some upper stage rocket bodies immediately deorbit the SOI and do not appear in our model, while other rocket bodies ($R(t)$) linger at the separation altitude and deorbit naturally at rate μ_R; these latter rocket bodies are inserted into the SOI at the annual rate λ_R. Although deorbiting of spacecraft and rocket bodies may actually take several months, sensitivity analysis (details not shown) reveals that our assumption of instantaneous deorbiting has a negligible impact on all of our results.

We assume passivation techniques (e.g., venting rocket bodies of residual fuel and discharging spacecraft batteries) are in place to prevent future explosions, and so debris is generated in our model only via collisions between satellites. Catastrophic collisions result in the fragmentation of both objects, whereas non-catastrophic collisions result in the fragmentation of the less massive object. Essentially all intact-intact collisions are catastrophic. We consider fragments having a characteristic length ≥ 10 cm, generally the lower limit of what sensors in the U.S. Space Surveillance Network can resolve (Johnson et al., 2001). We refer to fragments as hazardous or benign depending on whether or not they can produce catastrophic collisions with intacts; although fragments can be hazardous or benign to each other as well, this distinction is far less important because many fewer fragments are generated in fragment-fragment collisions. Hence, the effective fragment number is indexed by two symbols and will be written F_τ^κ, where $\kappa \in \{h, b\}$ refers to being hazardous or benign to intacts and $\tau \in \{R, S\}$ refers to the source of a fragment – rocket body or spacecraft. A particular fragment is not simply hazardous or benign to an intact: the uncertainty in collision velocity causes the properties of the fragment to determine the probability with which it is hazardous or benign in a particular collision. A particular fragment from source $\tau \in \{R, S\}$, therefore, increases the effective number of F_τ^h and F_τ^b by quantities that sum to one. Fragments deorbit at constant rate $\mu_{F_\tau^\kappa}$. To account for rocket body explosions or fragments entering the SOI from altitudes > 1000 km, we assume that new fragments arrive at rate $\lambda_{F_\tau^\kappa}$. Although we set $\lambda_{F_\tau^\kappa} = 0$ in our numerical com-

putations, we include this term to understand its impact in our equilibrium analysis.

Satellites of types α and γ participate in collisions at rate $\beta_{\alpha\gamma}\alpha(t)\gamma(t)$ at time t, where $\alpha, \gamma \in \{S, R, F_\tau^\kappa\}$. Because a satellite's cross section (which dictates its likelihood of collision) and mass (which determines the number of new fragments if it is involved in a collision) have a joint probability distribution, we cannot estimate in isolation the number of fragments resulting from a collision between two types of satellites. Rather, we assume that fragments of type F_τ^κ are generated from collisions between satellites of types α and γ at rate $\delta_{\alpha\gamma}^{\tau\kappa}\alpha(t)\gamma(t)$ at time t, for $\alpha, \gamma \in \{S, R, F_\tau^\kappa\}$ (a factor $\frac{1}{2}$ is necessary if $\alpha = \gamma$). For example, a collision between a rocket body and a spacecraft produces all four types of fragments: hazardous and benign fragments from both a rocket body and a spacecraft.

The effective number of spacecraft, hazardous fragments, benign fragments, and total fragments at time t are given by, respectively, $S(t) \equiv S_n^o(t) + S_n(t) + S_d(t)$, $F^h(t) \equiv F_R^h(t) + F_S^h(t)$, $F^b(t) \equiv F_R^b(t) + F_S^b(t)$, and $F^s(t) \equiv F^h(t) + F^b(t)$. Let $U \equiv \{S, R, F_S^h, F_S^b, F_R^h, F_R^b\}$ be the set of satellite types, $U^h \equiv \{S, R, F_S^h, F_R^h\}$ be the set of satellite types hazardous to intacts, $U^F \equiv \{F_S^h, F_S^b, F_R^h, F_R^b\}$ be the set of fragment types, and $U^I \equiv \{S, R\}$ be the set of intact types. The model is given by

$$\dot{R}(t) = \lambda_R - \sum_{\alpha \in U^h} \beta_{R\alpha} R(t)\alpha(t) - \mu_R R(t), \tag{1}$$

$$\dot{S}_n^o(t) = (1 - \theta_d)\lambda_o - \sum_{\alpha \in U^h} \beta_{S\alpha} S_n^o(t)\alpha(t) - \mu_o S_n^o(t), \tag{2}$$

$$\dot{S}_n(t) = \mu_o S_n^o(t) - \sum_{\alpha \in U^h} \beta_{S\alpha} S_n(t)\alpha(t) - \mu_n S_n(t), \tag{3}$$

$$\dot{S}_d(t) = \theta_d \lambda_o - \sum_{\alpha \in U^h} \beta_{S\alpha} S_d(t)\alpha(t) - \mu_o S_d(t), \tag{4}$$

$$\dot{F}_\tau^\kappa(t) = \lambda_{F_\tau^\kappa} + \frac{1}{2} \sum_{\alpha \in U} \sum_{\gamma \in U} \delta_{\alpha\gamma}^{\tau\kappa} \alpha(t)\gamma(t) - \mu_{F_\tau^\kappa} F_\tau^\kappa(t) \tag{5}$$

for $\tau \in U^I,\ \kappa \in \{h, b\}$.

A key shortcoming of the model relates to our handling of fragment-fragment collisions. We assume that a fragment generated in a fragment-fragment collision inherits the same properties as its ancestral intact (i.e., rocket body or spacecraft). That is, if we let the generation n of a fragment be the number of ancestors a fragment has that are fragments, then our model uses parameter values corresponding to collisions between only 0^{th}-generation fragments. This assumption is justifiable if there are few fragment-fragment collisions relative to collisions involving an intact satellite. But an orbital de-

bris environment in which a preponderance of collisions are between fragments will fill with n^{th}-generation fragments for large n, which do not pose as much of a hazard as 0^{th}-generation fragments.

Because the modeling of multiple generations of fragments would involve an enormous number of parameters, we instead view Eq. (5) as upper bounding the effect of fragment-fragment collisions, and then as a lower bound consider a variant of Eq. (5) that simply disregards fragment-fragment collisions, i.e., sets $\delta_{\alpha\gamma}^{\tau\kappa} = 0$ for $\alpha, \gamma \in U^F$. We will usually be ignoring fragment-fragment collisions. Hence, we refer to the version of the model with $\delta_{\alpha\gamma}^{\tau\kappa} > 0$ for $\alpha, \gamma \in U^F$ as the fragment-fragment version of the model; otherwise, the reader should assume that we are setting $\delta_{\alpha\gamma}^{\tau\kappa} = 0$ for $\alpha, \gamma \in U^F$. The intact-intact parameter values are the same in both versions of the model. When we ignore fragment-fragment collisions, the intact-benign fragment parameter values account only for the loss of a benign fragment, and the intact-hazardous fragment parameter values account only for the breakup of the intact and the loss of a hazardous fragment.

2.1 Equilibrium Analysis

For purposes of equilibrium analysis, we consider a simpler model that tracks only two types of satellites, intacts ($I(t)$) and hazardous fragments ($F(t)$):

$$\dot{I}(t) = -\beta_{II} I^2(t) - \beta_{IF} I(t) F(t) - \mu_I I(t) + \lambda_I, \tag{6}$$

$$\dot{F}(t) = \delta_{II} I^2(t) + \delta_{IF} I(t) F(t) - \mu_F F(t) + \lambda_F. \tag{7}$$

In §A, we define the parameters in Eqs. (6)-(7) in terms of the parameters in Eqs. (1)-(5) such that if $I(0) = I^s(0)$, where $I^s(t) = R(t) + S_n^o(t) + S_n(t) + S_d(t)$ is the total number of intacts in Eqs. (1)-(5), and $F(0) = F^s(0)$, then $F(t) \geq F^s(t)$ for $t \geq 0$; i.e., the number of hazardous fragments in Eqs. (6)-(7) provides an upper bound on the number of fragments in Eqs. (1)-(5).

In §A.3-A.4, we show that the hazardous fragments $F(t)$ in Eqs. (6)-(7) remain bounded and find an explicit expression for the equilibrium number of hazardous fragments in terms of the equilibrium number of intacts. The equilibrium number of intacts is given by the solution to a cubic equation if $\frac{\delta_{II}}{\beta_{II}} \neq \frac{\delta_{IF}}{\beta_{IF}}$ and by the solution to a quadratic equation if $\frac{\delta_{II}}{\beta_{II}} = \frac{\delta_{IF}}{\beta_{IF}}$; see §A.3 and §A.6. In addition, for the case $\theta_d = 1$ and $\lambda_R = 0$ (i.e., all space participants fully comply with deorbit procedures for rocket bodies and spacecraft), Eqs. (1)-(5) and Eqs. (6)-(7) are identical as $t \to \infty$ with identical parameters (e.g., $\delta_{IF} = \delta_{SF_S^h}^{Sh}$) with the exception that the factor $\frac{1}{2}$ is absorbed into the

parameter δ_{II}. Therefore, analytical results in §A.3 and §A.6 are exact for the most optimistic future.

Although we have performed an equilibrium analysis of the fragment-fragment version of the model, we do not include the analysis and only briefly comment on it here. The upper bounding of $F^s(t)$ in Eqs. (1)-(5) by $F(t)$ in Eqs. (6)-(7) still holds. There are two possibilities as $t \to \infty$: the number of hazardous fragments grows without bound, or the model approaches an equilibrium that is nearly identical to that of the model in which $\delta_{FF} = 0$ (this case occurs with our set of parameter values under full compliance).

2.2 Parameter Estimation

Values for the parameters in Eqs. (1)-(5) are estimated in §B using Monte Carlo integration, and appear in Tables B.1-B.4. Using the empirical probability distributions in Johnson et al. (2001), we assign each fragment a random characteristic length, area-to-mass ratio, and magnitude and direction of change in velocity after a collision; the first two random variables dictate a fragment's area and mass, while the third combines with the first two to give the hazard probability. In addition, each fragment's source's altitude is uniformly distributed within the SOI, and the direction of its post-collision change in velocity is uniformly distributed on the surface of the sphere. The collision rate parameters ($\beta_{\alpha\gamma}$), the debris generation parameters ($\delta^{\tau\kappa}_{\alpha\gamma}$), and the decay rates are computed by taking expectations over the three probability distributions from Johnson et al. (2001) and the two uniform distributions.

In the simulation, each fragment is weighted by the fraction of time it resides in the SOI, which is derived using the equations of orbital mechanics (e.g. King-Hele, 1964, Ch. 3). In addition, a fragment from source $\tau \in \{R, S\}$ is split between hazardous (F^h_τ) and benign (F^b_τ) by calculating the probability that a collision between it and an intact would be catastrophic, which occurs if the kinetic energy of the projectile in Joules is 40 times greater than the mass of the target in grams (Johnson et al., 2001).

To estimate the collision rate parameters, we use the ideal gas model (Alberty & Silbey, 1997) to derive an analytical expression for $\beta_{\alpha\gamma}$ in terms of the mean relative velocity of satellites in the SOI (Johnson et al., 2001), the volume of the SOI, and the mean collision cross sections of the various satellite types (using data from Kessler (2000) for intacts and the above probability distributions for fragments). We apply the ideal gas model to each portion of the SOI shell at a particular latitude, and use the full catalog of satellite element sets from Space Track (2008) to derive an empirical distribution of effective spatial density of satellites vs. latitude to capture the fact that the

spatial density of satellites – and hence the collision rate – is higher near the poles.

To estimate the debris generation parameters, we use Eq. (4) in Johnson et al. (2001), which specifies the number of fragments from a collision having characteristic length of at least a certain size, in terms of the mass of the two objects involved in the collision, the collision velocity, and whether the collision was catastrophic.

We estimate the decay rates as reciprocals of residence times. We set $\mu_o^{-1} =$ 3 yr to reflect the historical average of a 3-yr mission lifetime and the 25-yr decay rule recommended by NASA safety guidelines (NASA Safety Standard 1740.14, 1995; Liou & Johnson, 2005). To estimate μ_R, μ_n, and $\mu_{F_\tau^\kappa}$, we use data in Table 4 of Rossi et al. (1994) to equate the residence time of a satellite to 110 yr divided by the average area-to-mass ratio for the satellite type, which is quantified using the probability distributions in Johnson et al. (2001) for fragments and the values in Kaula (1983) for intacts.

To estimate the launch rate of new spacecraft into the SOI, we analyze the full catalog of satellite element sets at the end of 2007 from Space Track (2008), identify the satellites that were spacecraft, and determine the effective number of spacecraft in the SOI. Inspecting the annual launch rates of these spacecraft into the SOI over the past decade, we set $\lambda_o = 3$/yr. A similar analysis for rocket insertions leads to $\lambda_R = 1$/yr; because only a few rocket launchers remain that do not enable rocket body deorbiting, we assume $\lambda_R = 1$/yr for 10 years and $\lambda_R = 0$ thereafter. While the spacecraft deorbiting guidelines have been implemented, they have not been fully adopted by major space agencies (Liou & Johnson, 2007), and we set $\theta_d = \frac{2}{3}$ and perform a sensitivity analysis on θ_d later.

The full catalog of satellite element sets from Space Track (2008) are also used to determine the initial conditions $R(0)$, $S(0)$, and $F^s(0)$. We set $S_n^o(0) = \frac{(1-\theta_d)\lambda_o}{\mu_o}$ and $S_d(0) = \frac{\theta_d \lambda_o}{\mu_o}$ using Eq. (2) and Eq. (4), and $S_n(0) = S(0) - S_n^o(0) - S_d(0)$. To allocate $F^s(0)$ among the 4 fragment types, we assume that – aside from the FengYun 1C fragments, which are known to originate from a spacecraft – 90% of the initial fragments are from rocket bodies (our results are insensitive to this assumption) and use the simulated proportion of fragments of type F_τ^κ generated by the breakup of an intact.

2.3 Comparison to Liou & Johnson (2008)

NASA researchers have recently developed a 3-dimensional simulation of near-Earth orbital space that tracks each satellite over time (Johnson et al.,

2001; Liou & Johnson, 2005, 2008). Satellite breakups produce fragments whose properties are drawn from the distributions described in Johnson et al. (2001), though with some modifications as described in Liou & Johnson (2008). We compare the results of the fragment-fragment version of our model against those presented in Liou & Johnson (2008) for the SOI (private communication, Nicholas Johnson), which provide mean values for 150 200-yr simulation runs. We set $\lambda_o = \lambda_R = S_n^o(0) = S_d(0) = 0$ to coincide with the assumptions in Liou & Johnson (2008). The initial conditions evident in Fig. 8 of Liou & Johnson (2008) are $\approx$ 490 "intacts + mission related debris" and 520 fragments. It is not indicated what proportion of intacts are rocket bodies, nor is it clear what "mission related debris" constitutes. Because intact rocket bodies are larger and more spatially clustered (§B.2.3) than intact spacecraft, we must take care in determining our initial conditions for the comparison with Liou & Johnson (2008). The initial conditions we use in our (non-comparison) analysis are 207.2 spacecraft and 183.3 rocket bodies. In our initial conditions for the comparison, we set the initial number of rocket bodies to 183.3, the initial number of spacecraft to 490 - 183.3 = 306.7, and the initial number of fragments to 520, which are allocated among the 4 categories using the methods described earlier.

Fragment growth in both models is nearly linear for the first 200 years (Fig. A1), and our model underestimates the number of fragments after 200 years relative to Liou & Johnson (2008) by 8.6% (2356 vs. 2579). Our model overestimates the number of destroyed intacts (11.02 vs. 8.21) and the number of intact-intact collisions (4.38 vs. 2.65), underestimates the fraction of intact-fragment collisions that are catastrophic (0.33 vs. 0.44), and overestimates the fraction of fragment-fragment collisions that are catastrophic (0.81 vs. 0.67) (Table 1). Possible reasons for these discrepancies are given in §4.

3 Results

3.1 Base-Case Results

Numerical solutions to both versions of Eqs. (1)-(5) (Fig. 1) reveal that in both cases, the total number of fragments increases in a convex manner for $\approx$ 1500 yr. In the absence of fragment-fragment collisions, the total number of fragments approaches its asymptotic value ($F^s = 4.7 \times 10^5$, $F^h = 3.1 \times 10^5$), while in the presence of fragment-fragment collisions the number of fragments grows without bound, blowing up at time $t \approx 1473$ (although the fragment level remains bounded if we set $\theta_d = 1$; see Fig. A2). The two versions of the model are nearly indistinguishable for the first 500 yr (e.g., at 200 yr, $F^h(200) = 1006$ and 1015 in the absence and presence of fragment-fragment

collisions). Hereafter, we assume there are no fragment-fragment collisions.

The catastrophic intact-fragment collisions are the least frequent type of collision over the first several hundred years, but eventually become the most common type of collision (Fig. 2a,b). Our primary metric for measuring the hazard is the probability that a spacecraft launched at time t will be destroyed (via an intact-intact or catastrophic intact-fragment collision) while it is still operational, which is

$$r^o(t) = 1 - \left(1 - \sum_{\alpha \in U^h} \beta_{S\alpha} \alpha(t)\right)^{\mu_o^{-1}}. \tag{8}$$

This lifetime risk is initially 1.84×10^{-4} and increases to 2.82×10^{-4} in 200 yr (Fig. 2c). However, this risk rapidly increases in ≈ 1000 yr for ≈ 2000 yr, eventually approaching the equilibrium value of 2.19×10^{-2} (Fig. 2d).

3.2 Sensitivity Analyses

Because $\lambda_R > 0$ for only 10 yr in our model, our results are highly insensitive to the value of λ_R. We vary the spacecraft deorbit compliance rate θ_d while keeping the other parameters fixed at their base-case value (Fig. 3). While the lifetime risk to an operational spacecraft over the next 200 yr remains below 4.2×10^{-4} regardless of the value of θ_d, the sustainable lifetime risk decreases to 10^{-2} and 10^{-3}, respectively, if the deorbit compliance increases to 84.9% and 98.2%, respectively. The sustainable lifetime risk drops sharply for very high compliance rates and is 4.9×10^{-4} under full compliance (i.e., $\theta_d = 1$).

In the full compliance case, the fragment level peaks at 10,800, which is 11.3-fold higher than the current level (Fig. A2), after several millennia, and then approaches a very small equilibrium value ($F^s = 2.61$). Under full compliance, if the spacecraft launch rate is increased 10-fold (e.g., due to the emergence of reusable launch vehicles), then the lifetime risk in 200 yr is 2.53×10^{-4} and the sustainable lifetime risk is 9.05×10^{-4}.

3.3 On the Optimality of Full Deorbit Compliance

Motivated by the results of the sensitivity analyses, we compute the optimal compliance rate from a societal, sustainable perspective. Let C_d be the cost to deorbit, C_S be the cost of a destroyed operational spacecraft, θ_a be the attempted compliance rate, s be the probability that a deorbit attempt is successful (so that $\theta_d = s\theta_a$), and $r^o_{\max}(\theta_d)$ be the value of $\max_{t \geq 0} r^o(t)$ when the

successful compliance rate is θ_d. Then to minimize the sustainable costs related to spacecraft deorbiting and destruction, we solve $\min_{\theta_a} \theta_a C_d + r^o_{\max}(s\theta_a)C_S$.

We estimate the velocity requirements for deorbiting from the SOI to be Δv=128 m/s (§B.1.1). Extrapolating from the cost estimates in Table 3 of Wiedemann et al. (2004) (which are in FY 2002 dollars), the additional launch cost $\approx$ \$0.5M and the total development, production, and launch cost $\approx$ \$20M. We ignore the development and production cost, and assume the postmission deorbit cost is C_d = \$0.5M. The replacement cost of building and launching a new satellite is $\approx$ \$0.2-0.5B for a commercial, scientific, or weather satellite, or $\approx$ \$0.5-1.5B for a defense satellite (de Weck et al., 2003), and we set C_S = \$0.5B. The failure rate of propulsion systems has been estimated to be 3.9% (de Weck et al., 2003, Fig. 8), which yields $s = 0.961$. Substituting these values into the optimization problem and using the $r^o_{\max}(\theta_d)$ function in Fig. 3, we find that $\theta_a = 1$ is optimal.

To assess the robustness of this result, we determine how high the deorbit cost has to be to make $\theta_a = 1$ no longer optimal, which occurs when either the derivative of the total sustainable cost with respect to θ_a equals zero at $\theta_a = 1$, i.e., $C_d = -\frac{\partial r^o_{\max}(s\theta_a)}{\partial \theta_a}\Big|_{\theta_a=1} C_S$, or when the cost at $\theta_a = 0$ equals the cost at $\theta_a = 1$, i.e., $C_d = (r^o_{\max}(0) - r^o_{\max}(s))C_S$. The breakeven value is C_d = \$30.0M, which is 60 times larger than the actual value and several million dollars more than the total cost estimate in Wiedemann et al. (2004). Although we omit the details, a similar derivation shows that 100% compliance of rocket body deorbiting is also optimal.

3.4 Assessing the Damage due to Space Activities

A prerequisite for quantifying fees is to calculate the damage caused by various space activities. Toward this end, we define the damage caused by a space activity to be the total number of destroyed operational spacecraft generated by this activity. If we let $S^o(t) = S^o_n(t) + S_d(t)$ be the number of operational spacecraft at time t, then the number of destroyed operational spacecraft up to time T is

$$n_d(T) = \int_0^T S^o(t) \sum_{\gamma \in U^h} \beta_{S\gamma}\gamma(t)\ \mathrm{d}t. \tag{9}$$

Let $n_d^-(T)$ be the damage up to time T in the current environment, and n_d^+ be the damage up to time T after a perturbation has been applied at time 0. We define an activity's damage up to time T to be $n_d^+(T) - n_d^-(T)$. The perturbations are $R(0) \to R(0)+1$ for an extra rocket insertion, $R(0) \to R(0)-1$

and $F_R^\kappa(0) \to F_R^\kappa(0) + \frac{\hat{N}(1600)s_R^{R\kappa}}{2}$ for a rocket break up, and $S_n(0) \to S_n(0) - 1$ and $F_S^\kappa(0) \to F_S^\kappa(0) + \frac{\hat{N}(1600)s_S^{S\kappa}}{2}$ for a satellite break up, where the latter two perturbations follow from Eq. (B.44) and $\hat{N}(\cdot)$ and $s_\alpha^{\tau\kappa}$ are defined in Eqs. (B.40), (B.41), and (B.43). For a new extra launch, we do not want to consider the self-inflicted damage if the newly-launched spacecraft is destroyed while it is operational, although we do want to capture the subsequent damage caused by the fragments of such a collision. Hence, for a new extra launch of a spacecraft with deorbit capability, we add the equation $\dot{S}_d^u(t) = -\sum_{\alpha \in U^h} \beta_{S\alpha} S_d^u(t)\alpha(t) - \mu_o S_d^u(t)$ to Eqs. (1)-(5), let S_d^u be in the set U^h, and consider the perturbation $S_d^u(0) \to 1$ (from $S_d^u(0) = 0$). For a new extra launch of a spacecraft without deorbit capability, we simply set $S_n(0) \to S_n(0)+1$ because an operational spacecraft whose loss does not count as an operational loss can be considered inoperational from the very start.

The legacy cost is the difference between n_d in the current environment and n_d in an environment in which there are no nonoperational hazardous objects; i.e., we use the perturbation $F_\tau^\kappa(0) \to 0$, $S_n(0) \to 0$, and $R(0) \to 0$. In addition, we assess the portion of the legacy cost due to the FengYun 1C ASAT test via the perturbation $F_S^h(0) \to F_S^h(0) - 149.1$ and $F_S^b(0) \to F_S^b(0) - 251.8$ (§B.6).

The damage generated by a perturbation lasts for $\approx 10^4$ yr, and hence $n_d^+(T) - n_d^-(T)$ approaches a constant as $T \to \infty$ (Fig. 4). In the short term, a breakup produces more damage than an intact of the same type (Fig. 4); in the long term, the opposite is true because an intact remains in orbit longer than a fragment and so is hazardous for longer. In keeping with the sustainability philosophy (long time horizons are also considered for the nuclear waste depository at Yucca Mountain, which needs to comply for 10^4 yr (Long & Ewing, 2004)), we consider an infinite horizon and refer to the asymptotic value of $n_d^+(T) - n_d^-(T)$ as the damage. The damage from launching a spacecraft with deorbit capability is 2.15×10^{-5} destroyed spacecraft, which is 3000-fold less damaging than launching a spacecraft without deorbit capability. The FengYun 1C ASAT test can be expected to cause the same damage as 8 rocket body insertions or 2.6 launches of a spacecraft that does not deorbit, and constitutes 1.0% of the total legacy damage. In contrast, as a near-term practical problem, the ASAT test can be expected to cause the same damage over the next 100 years as 16.3 rocket body insertions or 41.1 launches of a spacecraft that does not deorbit, and is 5.8% of the total legacy damage.

Our damage calculations assume that the deorbit compliance rate θ_d and the launch rate λ_o do not change in the future. If there is a general consensus in how these parameters might change over time (e.g., θ_d increases from its current rate to a rate where the only noncompliance is due to propulsion system failures), then these predictions could be incorporated into the calculations. With the exception of rocket body insertions, the damage of the various

activities varies by $< 12\%$ for $\theta_d \in [0, 0.94]$ (Fig. A3).

3.5 Allocating the Legacy Damage

Finally, we consider the problem of attributing the total legacy damage to the various responsible parties (e.g., countries). Let $\rho_{i\gamma}$ be the proportion of objects of type $\gamma \in U^h$ having party i as their origin; we are not aware of any fragmentation event in which an object from one nation has been fragmented by an object from another, which allows us to assume that all fragments from an object owned by party i should be attributed to it. As usual, let γ itself be the number of objects of type γ. Finally, let ω_γ be the relative hazard of an object of type γ. The proportion of the total hazard that a party's objects contribute is $h_i \equiv \sum_{\gamma \in U^h} \omega_\gamma \rho_{i\gamma}$, and the absolute hazard attributed to party i is $h_i L$, where L is the total legacy damage.

The proportions $\rho_{i\gamma}$ must be determined by careful analysis of the present catalog, which is beyond the scope of this study. The relative hazard $\omega_\gamma = \frac{\tilde{\omega}_\gamma}{\sum_\gamma \tilde{\omega}_\gamma}$, where the hazard $\tilde{w}_\gamma$ is a physical property of a particular object type γ relative to the current orbital environment, and can be calculated as the partial derivative of n_d with respect to an object type γ:

$$\tilde{\omega}_\gamma = \frac{\partial n_d}{\partial \gamma} \approx \frac{n_d(\gamma + \delta_\gamma) - n_d(\gamma)}{\delta_\gamma}, \tag{10}$$

where the argument of n_d indicates what is varied. We set $\delta_\gamma = 1$ (although the results are insensitive to δ_γ; 0.01 and 1 produce essentially the same hazards), so that $\tilde{\omega}_\gamma$ coincides with the quantity $n_d^+ - n_d^-$ defined earlier. We consider an infinite horizon and find that the relative hazard is 0.239 for rocket bodies, 0.739 for spacecraft that do not deorbit, 0.009 for hazardous rocket body fragments, and 0.013 for hazardous spacecraft fragments. Using the initial conditions in §B.6 and these values, we find that 22.7%, 75.7%, 0.5%, and 1.1% of the total legacy damage is due to intact rocket bodies, intact spacecraft, hazardous rocket body fragments, and hazardous spacecraft fragments, respectively.

4 Discussion

4.1 The Model

Eqs. (1)-(5) attempt to capture the mean behavior of a three-dimensional object-by-object simulation such as LEGEND (Liou et al., 2004) and other

models of similar complexity (Sdunnus et al., 2004). Compared to most previous ODE models (Farinella & Cordelli, 1991; Kessler, 2000; Rossi et al., 1994) (a notable exception is Rossi et al. (1998), which considers a large number of ODEs, one for each triple of semimajor axis, eccentricity, and satellite mass), ours is distinctive in that we estimate parameters by taking expectations of empirical distributions, we introduce separate tracking of hazardous and benign fragments, which makes sense given their different mean characteristics, and we introduce the nonuniformity factor that captures the higher collision rates near the poles. Although our model appears at first glance to be much simpler than the simulation models in Liou et al. (2004) and Sdunnus et al. (2004), its complexity is in calculating parameter values, which are expectations over the same distributions that govern an object-by-object simulation. The advantages of our approach are enumerated below.

A comparison to results in Liou & Johnson (2008) (which uses LEGEND) shows that our model generates qualitatively similar results (Fig. A1 and Table 1), although any number of physical phenomena and simple accounting differences could explain the discrepancies. These include: differences in assumed characteristics of intact spacecraft and rocket bodies (we assume all spacecraft and rocket bodies have the same mass and take the average area and mass of a satellite from Kessler (2000) because Liou & Johnson (2008) does not provide the relevant quantities); different initial conditions (our knowledge of the initial conditions used in Liou & Johnson (2008) is quite limited); we use mean values to determine the effects of collisions, whereas each collision in Liou & Johnson (2008) is different; the cost of neglecting fragments from fragmentation events occurring outside the SOI – though fragments from above decay slowly, eccentric fragments would immediately enter the SOI; the error made in assuming that intact-intact collisions occur according to a chemical kinetics model (in particular, intacts may originally have been placed in nonconflicting orbits, whereas the chemical kinetics model assumes a particle is placed in a trajectory independent of the positions of any of the other particles); different orbital decay behavior; and rocket bodies are allowed to explode during the first 10 years of the simulation in Liou & Johnson (2008).

There are several advantages to using a simple ODE model such as Eqs. (1)-(5) rather than a complex simulation model: it runs almost instantaneously, which elucidates asymptotic behavior (Kessler, 2000) and eases the sensitivity analysis task (once the parameters are calculated, one can quickly compute many derived quantities that depend on perturbations in mean behavior, whereas it would be necessary to run a computationally intensive object-by-object simulation repeatedly to obtain mean behavior, and then repeat this for each desired perturbation); it allows a level of transparency and understanding that could be valuable if, e.g., multiple countries need to coalesce around a set of damage estimates; and it is amenable to rigorous analytical results involving asymptotic behavior. Our model is generic and can be used at other

altitudes, although the space discretization may need to be smaller at lower altitudes to account for the higher sensitivity of escape rate with altitude, and it may be less accurate at altitudes that have considerable congestion at shells just above it (unlike the SOI, see Fig. 7 in Liou & Johnson (2008)).

4.2 Results

Although our model and analysis have some similarities with previous research, and our numerical results appear to be similar to that of previous research, we come to different conclusions, both in terms of analytical results and policy implications. In terms of analysis, if we interpret the results in Kessler (2000) in terms of our Eqs. (6)-(7), it claims that $F(t)$ grows without bound if $I(t) > \frac{\mu_F}{\delta_{IF}}$, which is referred to as the "runaway threshold". If we set $\lambda_F = 0$ (as in Kessler (2000)), then the nullcline $F(I)$ (derived by setting $\dot{F}(t) = 0$ Eq. (7) and solving for I; see Eq. (A.18)) is

$$F(I) = \frac{\delta_{II} I^2}{\mu_F - \delta_{IF} I}, \tag{11}$$

which coincides with Eq. (3) in Kessler (2000). The discrepancy between our claim that $F(t)$ is always bounded and the result in Kessler (2000) is that the number of intacts I in the numerator of Eq. (11) is treated as a constant in Kessler (2000), whereas we capture via Eq. (6) the dynamic interaction between I and F (i.e., intacts decrease as fragments increase).

More importantly, while our numerical results mimic earlier results (Liou & Johnson, 2005; Walker & Martin, 2004) that stressed the importance of postmission deorbiting, we do not necessarily agree with the claim that the only way to prevent future problems is to remove existing large intacts from space (Liou & Johnson, 2006, 2008). The divergence between our views and those in Liou & Johnson (2006, 2008) is perhaps due to the different performance metrics used. The root causes for alarm in Liou & Johnson (2006, 2008) appear to be the growth rate of fragments and the small increase in the rate of catastrophic collisions over the next 200 years (Liou & Johnson, 2008, Fig. 2). However, the great majority of catastrophic collisions in the SOI do not involve operational spacecraft, and are hazardous only in the sense that the fragments generated from such a collision could subsequently damage or destroy operational spacecraft. Therefore, we introduced the notion of the lifetime risk of an operational spacecraft as the primary performance metric. When viewed from this lens, our model predicts that the lifetime risk is $< 5 \times 10^{-4}$ over the next two centuries, and always stays $< 10^{-3}$ if there is very high ($> 98\%$) spacecraft deorbiting compliance. These risks appear to be low relative to the immense cost and considerable technological uncertainty involved in removing large objects from space, are dwarfed by the $\approx 20\%$ his-

torical mission-impacting (but not necessarily mission-ending) failure rate of spacecraft (Frost & Sullivan, 2004), and could be overestimated if improved traffic management techniques lower future collision risks (Johnson, 2004). Hence, the need to bring large objects down from space does not appear to be as clear cut as suggested in Liou & Johnson (2006, 2008). Nonetheless, our model does not incorporate the possibility of intentional catastrophic collisions (ASAT tests, space wars) that could conceivably occur in the future. In addition, Fig. 3 considers only catastrophic collisions, whereas noncatastrophic intact-fragment collisions could easily disable an operational spacecraft. If the operational lifetime risk is modified to include noncatastrophic collisions with fragments ≥ 10 cm, then the sustainable risk rises by $\approx 50\%$: it increases from 2.19×10^{-2} to 3.09×10^{-2} in the base case, and increases from 4.91×10^{-4} to 7.94×10^{-4} in the full compliance case. Moreover, if fragments ≥ 1 cm (rather than ≥ 10 cm) are harmful to spacecraft (Johnson, 2004), then we (as well as other researchers) could be underestimating the risk.

In summary, in the absence of the removal of large objects from space, the sustainable lifetime risks in Figs. 2-3 do not appear to be obviously above or below a tolerable level. Even if these risks are deemed acceptable, it is prudent to invest in research and development for space remediation technologies, which is a topic of current study (Proposal for forming an IAA study group, 2000). However, given the optimality of full deorbit compliance from a societal, sustainable perspective, and the sensitivity of sustainable lifetime risk to postmission deorbit compliance, the primary focus for policymakers should be on increasing compliance, which leads us to a discussion of economic instruments that could be used to address this issue.

4.3 Setting Fees

Creating a set of viable economic instruments will be extremely difficult, and requires sustained political negotiations by a large number of actors; here, we simply discuss some of the key challenges that would be faced in transforming the damages in Fig. 4 into specific fees that could be imposed on past and future debris-generating activities. Such fees are consistent with the "polluter pays" principle proposed to address global climate change (Claussen & McNeilly, 1998).

At a strategic level, the first challenge is to decide what types of activities to tax, and for what reasons. One reason to charge a fee is to deter future debris-generating activity (i.e., ideally no fees are collected for certain activities), while another reason could be to generate funds for, e.g., compensating owners of operational spacecraft that are victims of future catastrophic collisions (which are largely random events), subsidizing postmission deorbiting,

or performing research and development into various mitigation technologies (e.g., methods that remove large objects from space, electric propulsion systems that could reduce the cost of deorbiting (Ryden, 1997), improved space traffic management techniques (Johnson, 2004), and spacecraft shielding).

We begin with the most benign activity, which is the launching of a spacecraft that deorbits after its mission. Because this spacecraft is doing its best to preserve space, one might argue that it should only be charged a fee that compensates for its future expected damage. In this case, the damage that occurs at time t should be multiplied by e^{-rt} inside the integral in Eq. (9), where r is the discount rate, and the total discounted damage should be multiplied by the replacement cost of a satellite. As an illustrative example, if we set $r = 0.05$ (Perman et al., 2003) and $C_S = \$0.5B$, then the launch fee is only \$980 (for implementation, the values of r and C_S need to be estimated with considerable care and achieve broad consensus).

Note that a noncompliance fee for spacecraft that do not deorbit can be viewed as using differential launch fees that depend on whether or not a spacecraft deorbits. The primary motivation of a noncompliance fee is to preserve space (Fig. 3). To produce a deterrent effect, the fee to launch a spacecraft that does not deorbit needs to be at least the deorbit cost plus the fee (if any) to launch a spacecraft that deorbits. The voluntary guideline, which implies that it is better to incur a deorbit cost now rather than destroy 0.065 spacecraft in the future, according to our calculations, has not achieved full compliance. It is important to understand the reasons for the current deorbit noncompliance, which could shed light on how to improve compliance. If players are acting rationally and in their own self-interest, then possible reasons for not deorbiting are (i) they are behaving myopically and are discounting collisions that happen far in the future, perhaps having faith in a future technological solution to the problem; (ii) they do not plan many future launches in congested regions of space (such as the SOI), and so will not receive the benefits (i.e., avoided future collisions) from deorbiting; and (iii) they have an inventory of old spacecraft that are expensive to retrofit for deorbiting. To the extent that different players have different (perceived) deorbit costs and benefits, the noncompliance fee (or deorbit subsidy) needs to be sufficiently high to deter all players. If the fee is to be based on damages and if a single player (i.e., space agency) can substantially alter θ_d by his postmission deorbit policy, then it may be more appropriate to assess the damage of his aggregate policy decision.

Another challenge for a noncompliance fee stems from the moral hazard issue: the failure rate of propulsion systems has been estimated to be 3.9% (de Weck et al., 2003, Fig. 8), and hence even if a spacecraft owner plans to deorbit after the mission is complete, he may fail to do so, and the international space community may have no way of verifying whether the failure to deorbit was

deliberate or intentional. The fee structure would have to address this issue. Much of the above discussion about a deorbit noncompliance fee also holds for failing to deorbit rocket bodies or failing to follow passivation techniques, although compliance for these activities appears to be much closer to 100% than spacecraft deorbiting.

There is also a legacy issue, which typically arises when discussing launch costs (Prasad, 2005, e.g.), in that most of the satellites in LEO were launched by a small group of countries. Hence, there could also be a one-time legacy fee due to all existing space objects currently in the SOI. The use of legacy fees is a particularly thorny political issue related to, e.g., the Cold War and the original research and development costs incurred by the U.S. and U.S.S.R. that subsequent countries did not bear. Sustainability is a modern goal and during the Cold War (when much of the existing debris was generated), the U.S. and U.S.S.R. were not concerned with preserving space for the future. It is also not clear to what extent Russia feels responsible for past U.S.S.R. behavior. In any case, these activities are in the past and not deterable. If one wanted to charge a one-time legacy cost to cover future expected damages, then (using $r = 0.05$ and $C_S = \$0.5\text{B}$) the legacy fee is \$5.55M. To allocate this fee across various players, the relative hazards ($\tilde{\omega}_\gamma$) should also be computed with $r = 0.05$, which yields 0.618 for rocket bodies, 0.236 for spacecraft that do not deorbit, 0.077 for hazardous rocket body fragments, and 0.068 for hazardous spacecraft fragments; combining these numbers with the initial conditions, we find that the total legacy damage due to these 4 satellite types is 63.0%, 26.0%, 4.6%, and 6.4%, respectively.

ASAT tests are another politically-charged issue. The FungYun 1C ASAT test may have been partially motivated by former U.S. and Soviet ASAT tests and by the U.S. December 2001 withdrawal from the Anti-Ballistic Missile treaty. As with a deorbit noncompliance fee, the primary goal of an ASAT test fee would be as a deterrent. In contrast to the case where there is a failure to deorbit, it is difficult to determine the magnitude of a financial deterrent because it is very difficult to put a financial cost on the value (to the tester) of an ASAT test. The ASAT test fee might be set to significantly exceed its damage so as to discourage the militarization of space, essentially charging it not only for its test but for the escalation effect it may have on other players.

4.4 Conclusion

It appears that if full compliance of the 25-yr spacecraft deorbiting guidelines can be achieved within the next few decades and no ASATs are used or tested in the future, then the lifetime risk from space debris in the SOI may be sustainable at a tolerable ($\approx 10^{-3}$) level. Hence, the focus of policy should

be on achieving full deorbit compliance (including improving the reliability of propulsion systems) and fostering a culture that makes ASAT tests (and use) taboo. Indeed, at the current launch rate of 3/yr and a deorbit cost of $0.5M, the total undiscounted deorbit cost after 1000 years is $1.5B, which is the cost of launching a single defense spacecraft. It seems improbable that a future technology will be able to clean up space for less cost than launching a single defense spacecraft. Our analysis also provides a framework for setting fees for past and future space activities, but many challenges remain in developing a viable set of economic instruments.

Acknowledgment. This research was supported by the Center for Social Innovation, Graduate School of Business, Stanford University (L.M.W.) and by a Scott A. and Geraldine D. Macomber Stanford Graduate Fellowship and a National Science Foundation Fellowship (A.M.B.). We thank Jeremy Bulow, Lawrence Goulder, Nicholas Johnson, and Erica Plambeck for helpful conversations, and Nicholas Johnson for sharing the data in Table 1.

References

Alberty, R.A., & Silbey, R.J, *Physical chemistry*, 2nd edition, John Wiley and Sons (New York, NY, 1997).

Claussen, E., & McNeilly,L., Equity & global climate change: the complex elements of global fairness. Pew Center on Global Climate Change, October 29, 1998. Accessed at http://www.pewclimate.org/global-warming-in-depth/all_reports/equity_and_climate_change on May 20, 2008.

Farinella, P., Cordelli, A., The proliferation of orbiting fragments: A simple mathematical model, *Science and Global Security* 2, 365-378, 1991.

Frost & Sullivan. Commercial communications satellite bus reliability analysis, August 2004. Accessed at http://www.satelliteonthenet.co.uk/white/-frost3.html on June 3, 2008.

Guidelines and Assessment Procedures for Limiting Orbital Debris, NASA Safety Standard 1740.14, NASA Office of Safety and Mission Assurance, August 1995.

Johnson, N.L., Space traffic management: concepts and practices. *Space Policy*, 20, 79-85, 2004.

Johnson, N.L, Krisko, P.H., Liou, J.-C., & Anz-Meador, P.D, NASA's new breakup model of EVOLVE 4.0, *Advances in Space Research*, 28, 1377-1384, 2001.

Kaula, W.M., *Theory of satellite geodesy: applications of satellites to geodesy.* Yale University Press (New Haven, CT, 1983).

Kessler, D.J., Critical density of spaceraft in Low Earth Orbit: using fragmentation data to evaluate the stability of the orbital debris environment.

Johnson Space Center report #28949, NASA and LMSEAT Report #33303, Lockheed Martin, February 2000.

King-Hele, D., *Theory of satellite orbits in an atmosphere*. Blackie, Glascow and London, 1964.

Liou, J.-C., Hall, D.T., Krisko, P.H., & Opiela, J.N., LEGEND - a three-dimensional LEO-to-GEO debris evolutionary model. *Advances in Space Research*, 34, 981-986, 2004.

Liou, J.-C., & Johnson, N.L., A LEO satellite postmission disposal study using LEGEND. *Acta Astronautica*, 57, 324-329, 2005.

Liou, J.-C., & Johnson, N.L., Risks in space from orbiting debris, *Science*, 311, 340-341, 2006.

Liou, J.-C., & Johnson, N.L., A sensitivity analysis of the effectiveness of active debris removal in LEO, Paper IAC-07-A6.3.05, International Astronautical Congress, Hyderabad, India, September 2007. Accessed at http://ntrs.nasa.gov/archive/nasa/casi.ntrs.nasa.gov/-20070013702_2007011170.pdf on December 17, 2007.

Liou, J.-C., & Johnson, N.L., Instability of the present LEO satellite populations, *Advances in Space Research*, 41, 1046-1053, 2008.

Liou, J.-C., & Portman, S., Chinese anti-satellite test creates most severe orbital debris cloud in history, *Orbital Debris Quarterly News*, 11, Issue 2, April 2007.

Long, J.C.S., & Ewing, R.C., Yucca Mountain: earth-science issues at a geologic repository for high-level nuclear waste, *Annual Reviews Earth Planetary Science* 32, 363-401, 2004.

Perman, R., Ma, Y., McGilvray, J., & Common, M., *Natural resource and environmental economics*, 3rd edition, Pearson Education Ltd (Harlow, UK, 2003).

Prasad, M.Y.S., Technical and legal issues surrounding space debris - India's position in the UN, *Space Policy*, 21, 243-249, 2005.

Proposal for forming an IAA study group, IAA, Paris, October 2000 http://iaaweb.org/iaa/Scientific%20Activity/Study%20Groups/-SG%20Commission%205/sg55/s55.pdf, accessed on June 10, 2008.

Rossi, A., Energetic cost and viability of the proposed space debris mitigation measures, *J. Spacecraft Rockets*, 39, 540-550, 2002.

Rossi, A., Anselmo, L., Cordelli, A., Farinella, P., & Pardini, C.. Modelling the evolution of the space debris population, *Planetary Space Science*, 46, 1583-1596, 1998.

Rossi, A., Cordelli, A., Farinella, P., & Anselmo, L., Collisional evolution of Earth's orbital debris cloud, *Journal Geophysical Research*, 99, 23195-23210, 1994.

Ryden, K.A., Fearn, D.G., & Crowther, R., Electric propulsion: a solution to end-of-life disposal of satellites? *Proc. second European conference on space debris*, W. Flury (Ed), ESA, Noordwijk, Netherlands, 709-712, 1997.

Sdunnus, H., Beltrami, P., Klinkrad, H., Matney, M., Nazarenko, A., & Wegener, P., Comparison of debris flux models, *Advances in Space Research*,

34, 1000-1005, 2004.
Soroos, M.S., The commons in the sky: the radio spectrum and geosynchronous orbit as issues in global policy, *International Organization*,36, 665-677, 1982.
Space track, http://www.space-track.org, accessed on April 30, 2008.
Walker, R., Martin, C.E., Cost-effective and robust mitigation of space debris in low Earth orbit, *Advances in Space Research*, 34, 1233-1240, 2004.
de Weck, O., de Neufville, R., Chang, D., & Chaize, M., Technical success and economic failure, unit 1 of Communications satellite constellations, Engineering Systems Learning Center, MIT, Cambridge, MA, October 14, 2003. Accessed at http://ardent.mit.edu/real_options/-de%20Weck%20System%20Study/unit1_summary.pdf on June 2, 2008.
Wiedemann, C., Krag, H., Bendisch, J., & Sdunnus, H., Analyzing costs of space debris mitigation methods, *Advances in Space Research*, 34, 1241-1245, 2004.

A Equilibrium Analysis

We perform an equilibrium analysis of Eqs. (6)-(7) in §A and estimate the parameters for Eqs. (1)-(5) in §B. In addition, Figs. A1-A3 provide supporting numerical results that are discussed in the main text.

In §A.1, we examine the relationship between Eqs. (1)-(5) and Eqs. (6)-(7). Although we have analyzed the case with fragment-fragment collisions and summarized our key findings in the main text, in this presentation we assume the fragment-fragment collision parameters are zero. Our objective in the remainder of this section is to characterize the equilibrium points (EP), also called steady-state solutions, for Eqs. (6)-(7). In §A.2, we solve for the equilibrium value of I in terms of the equilibrium value of F. In §A.3-A.6, we prove existence and uniqueness of an EP, show that the number of fragments is bounded, and obtain a closed-form solution to Eqs. (A.11)-(A.12) in the case when $\frac{\delta_{II}}{\beta_{II}} = \frac{\delta_{IF}}{\beta_{IF}}$. Throughout our analysis, we assume $\beta, \delta, \mu > 0$.

A.1 Bounding Properties of Eqs. (6)-(7)

In this subsection, we show that under a specified relationship between the parameters of Eqs. (1)-(5) in the main text and those in Eqs. (6)-(7) in the main text, the number of fragments in the latter model provides an upper bound on the number of fragments in the former model.

Let the parameters in Eqs. (6)-(7) be related to those in Eqs. (1)-(5) via

$$\beta_{II} = \max \beta_{\alpha\gamma}, \tag{A.1}$$
$$\beta_{IF} = \max \beta_{\alpha\zeta}, \tag{A.2}$$
$$\mu_I = \min\{\{\text{if } \lambda_R > 0,\ \mu_R;\ \text{else } \infty\}, \tag{A.3}$$
$$\{\text{if } \theta_d < 1,\ \mu_n;\ \text{else } \infty\}, \mu_o\}, \tag{A.4}$$
$$\lambda_I = \lambda_R + \lambda_o, \tag{A.5}$$
$$\frac{\delta_{II}}{\beta_{II}} = \frac{\delta_{IF}}{\beta_{IF}} = \max\left\{\max \frac{\delta^{\tau\kappa}_{\alpha\gamma}}{2\beta_{\alpha\gamma}}, \max \frac{\delta^{\tau\kappa}_{\alpha\zeta}}{\beta_{\alpha\zeta}}\right\}, \tag{A.6}$$
$$\mu_F = \min \mu_\zeta, \tag{A.7}$$
$$\lambda_F = \sum \lambda_\zeta, \tag{A.8}$$

for $\alpha, \gamma \in U^I$, $\zeta, \eta \in U^F$, $\tau \in \{R, S\}$, $\kappa \in \{h, b\}$.

If we neglect collisions, the number of intacts of each type follows linear first-order equations, and hence exponentially approaches – starting from its initial conditions – the following equilibria:

$$\begin{aligned}
R(t) &\to \frac{\lambda_R}{\mu_R}, \\
S^o_n(t) &\to \frac{(1-\theta_d)\lambda_o}{\mu_o}, \\
S_n &\to \frac{(1-\theta_d)\lambda_o}{\mu_n}, \\
S_d &\to \frac{\theta_d \lambda_o}{\mu_o}, \\
I &\to \frac{\lambda_I}{\mu_I}.
\end{aligned} \tag{A.9}$$

Because collisions decrease the number of intacts, it follows that the number of intacts is bounded in both models.

Let $I^s(t) \equiv R(t) + S^o_n(t) + S_n(t) + S_d(t) + S^u_d(t)$ be the total number of intacts in Eqs. (1)-(5), and recall that $F^s(t) = F^h_R(t) + F^b_R(t) + F^h_S(t) + F^b_S(t)$ is the total number of hazardous fragments in this model. We show that if $I(0) = I^s(0)$ and $F(0) = F^s(0)$, then

$$F(t) \geq F^s(t) \quad \text{for} \quad t \geq 0. \tag{A.10}$$

Assume $I(0) = I^s(0)$. Suppose there is a time $t_2 > 0$ at which $F(t_2) < F^s(t_2)$. Consider the latest time $t_1 \in [0, t_2)$ at which $F(t_1) = F^s(t_1)$. Let I_c be the number of destroyed intacts up to time t_1 in Eqs. (6)-(7) and I^s_c, the number in Eqs. (1)-(5). Because $\mu_I \leq \mu_o$ and $\lambda_I \geq \lambda_o$ by Eqs. (A.4)-(A.5), $I(t) + I_c(t) \geq I^s(t) + I^s_c(t)$ for $t \geq 0$. By Eq. (A.6), the number of fragments emerging from a destroyed intact in Eqs. (6)-(7) exceeds the number emerging

from one in Eqs. (1)-(5), regardless of the collision mechanism. Furthermore, by Eq. (A.7), fragments in Eqs. (6)-(7) decay no faster than in Eqs. (1)-(5). Therefore, if $F(t_1) = F^s(t_1)$, then $I_c(t_1) \leq I_c^s(t_1)$. Combining this with Eq. (A.10) yields $I(t_1) \geq I^s(t_1)$. But then $\dot{F}(t_1) \geq \dot{F}^s(t_1)$, and so t_1 is not the latest time before t_2 at which $F(t) = F^s(t)$. This is a contradiction, which completes the proof of Eq. (A.10).

We already showed that $I^s(t)$ is bounded above. Eqs. (6)-(7) is simple enough to enable an asymptotic analysis and, according to Eq. (A.10), gives an upper bound on the asymptotic behavior of $F^s(t)$. If Eqs. (6)-(7) has a stable equilibrium point, then Eqs. (1)-(5) has a stable equilibrium point at which $F^s \leq F$. For consider an initial condition $(I(0), F(0))$ that starts a trajectory ending at a stable equilibrium point. When started with the same initial condition, with the number of intacts I distributed by any means among the various intact types in Eqs. (1)-(5), Eqs. (1)-(5) in the main text must produce a trajectory along which I^s is bounded and, according to Eq. (A.10), $F^s \leq F$. Hence, Eqs. (1)-(5) has a stable equilibrium point too.

Finally, consider the case $\theta_d = 1$ and $\lambda_R = 0$, i.e., a future in which all space participants comply 100% with deorbit procedures for rocket bodies and spacecraft. In the limit $t \to \infty$, $R(t) \to 0$, $S_n^o(t) \to 0$, $S_n(t) \to 0$, and $F_R^\kappa(t) \to 0$. In this case, in the limit $t \to \infty$, Eqs. (1)-(5) and (6)-(7) are exactly the same, and the parameter values may be identified with each other without taking extrema in Eqs. (A.1)-(A.4), (A.6)-(A.7).

A.2 Suitable equilibrium points

We set $\dot{I}(t) = \dot{F}(t) = 0$ in Eqs. (6)-(7) and analyze

$$-\beta_{II} I^2 - \beta_{IF} IF - \mu_I I + \lambda_I = 0, \tag{A.11}$$
$$\delta_{II} I^2 + \delta_{IF} IF - \mu_F F + \lambda_F = 0. \tag{A.12}$$

Eqs. (6)-(7) have the form $\dot{y}(t) = fy(t) + g$, where $g \geq 0$ and does not contain y. Therefore, if $(I(0), F(0)) \geq 0$ then $(I(t), F(t)) \geq 0 \ \forall t \geq 0$. By Eq. (A.9), we are interested in an EP $(I^{\text{ss}}, F^{\text{ss}})$ such that $I^{\text{ss}} \in \left[0, \frac{\lambda_I}{\mu_I}\right] \equiv \mathcal{I}$ and $F^{\text{ss}} \geq 0$. We call such an EP satisfying these conditions *suitable*.

We first show that if F^{ss} exists, then $I^{\text{ss}} \in \mathcal{I}$ and so is suitable. Suppose $F \geq 0$. If we write Eq. (A.11) as

$$q(I) \equiv -\beta_{II} I^2 - (\beta_{IF} F + \mu_I) I + \lambda_I = 0, \tag{A.13}$$

then $q(0) = \lambda_I \geq 0$, $q\left(\frac{\lambda_I}{\mu_I}\right) = -\lambda_I^2\mu_I^{-2}\beta_{II} - \lambda_I\mu_I^{-1}\beta_{IF}F \leq 0$, and $\lim_{I\to\pm\infty} q(I) = -\infty$. Hence $q(I)$ has one zero no greater than $I = 0$ and one zero in the interval $\mathcal{I}$ and so $I^{\text{ss}} \in \mathcal{I}$. It follows that

$$I = \frac{-\beta_{IF}F - \mu_I + \sqrt{(\beta_{IF}F + \mu_I)^2 + 4\lambda_I\beta_{II}}}{2\beta_{II}}. \tag{A.14}$$

A.3 Existence

For convenience, we define $\Delta \equiv \frac{\delta_{II}}{\beta_{II}} - \frac{\delta_{IF}}{\beta_{IF}}$. The solution to Eqs. (A.11)-(A.12) is

$$F(I) = \frac{\lambda_F + \frac{\delta_{II}}{\beta_{II}}(\lambda_I - \mu_I I)}{\mu_F + \Delta\beta_{IF}I}, \tag{A.15}$$

where I satisfies the cubic equation

$$\begin{aligned} g(I) = &-\Delta\beta_{II}\beta_{IF}I^3 + \left(-\mu_F\beta_{II} - \mu_I\Delta\beta_{IF} + \mu_I\frac{\delta_{II}}{\beta_{II}}\right)\beta_{IF}I^2 \\ &+(\lambda_I\Delta\beta_{IF} - \mu_F\mu_I - \lambda_I D_{II}\beta_{IF} - \lambda_F\beta_{IF})I + \lambda_I\mu_F = 0. \end{aligned} \tag{A.16}$$

We now show that Eqs. (A.11)-(A.12) have a unique suitable EP. We have already shown that if $F^{\text{ss}} \geq 0$ exists, then $I^{\text{ss}} \in \mathcal{I}$. Solving Eqs. (A.11)-(A.12) for F yields the nullclines

$$F_1(I) = \frac{\lambda_I - \mu_I I - \beta_{II}I^2}{\beta_{IF}I}, \tag{A.17}$$

$$F_2(I) = \frac{\lambda_F + \delta_{II}I^2}{\mu_F - \delta_{IF}I}. \tag{A.18}$$

The intersection of these nullclines is an EP.

For $I \geq 0$, $F_1(I)$ is monotonically decreasing in I, $\lim_{I\to 0^+} F_1(I) = +\infty$, and $F_1(I) = 0$ if

$$I = I^\dagger \equiv \frac{-\mu_I + \sqrt{\mu_I^2 + 4\lambda_I\beta_{II}}}{2\beta_{II}}. \tag{A.19}$$

We note that $0 \leq I^\dagger \leq \frac{\lambda_I}{\mu_I}$, where the latter inequality holds because $F_1\left(\frac{\lambda_I}{\mu_I}\right) \leq 0$.

If we define

$$I^\star = \frac{\mu_F}{\delta_{IF}}, \tag{A.20}$$

then $F_2(0) = \frac{\lambda_F}{\mu_F}$, $\lim_{I \to I^\star} F_2(I) = +\infty$, $F_2(I)$ is monotonically increasing for $I < I^\star$, and $F_2(I) < 0$ for $I > I^\star$. These properties show that $F_1(I)$ and $F_2(I)$ intersect exactly once at a point satisfying $F^{\text{ss}} \geq 0$.

A.4 Growth of Fragments

In this subsection, we show that $F(t)$ is bounded above. To begin our argument, we consider $q(I)$ defined by Eq. (A.13) for a fixed F. The analysis below Eq. (A.13) shows that there exists a unique $I^\star \in \mathcal{I}$ such that $q(I^\star) = 0$. In addition, Eq. (A.13) implies that $q'(I) = -2\beta_{II} I - \beta_{IF} F - \mu_I < 0$, i.e., the EP $I^\star$ is asymptotically stable. Because $I^\star$ is a unique EP that is asymptotically stable, and I is bounded above, it follows that

$$\text{all trajectories approach } I^\star \text{ asymptotically.} \tag{A.21}$$

Furthermore, the solution to Eq. (A.13) given in Eq. (A.14) implies that

$$\text{if } \; F_2 > F_1, \text{ where } F_1 \text{ and } F_2 \text{ are constant, then } I_2^\star < I_1^\star. \tag{A.22}$$

We now suppose that $F(t)$ increases without bound, and find a contradiction. Then there exists a time t_1 beyond which $F(t) \geq F_1$. Set $F(t)$ equal to F_1 in Eq. (A.13). Statement (A.22) implies that $I^\star(F_1) \geq I^\star(F(t))$ for $t \geq t_1$. This and statement (A.21) imply that for any $\varepsilon > 0$ there exists a time t_2 beyond which $I(t) \leq (1+\varepsilon) I^\star(F_1) \equiv I_1$.

This last inequality implies that in our ODE $\dot{F}(t) = \delta_{II} I^2(t) + (\delta_{IF} I(t) - \mu_F) F(t) + \lambda_F$, for $t \geq t_2$ we have the inequality $\delta_{IF} I - \mu_F \leq \delta_{IF} I_1 - \mu_F \equiv -b_F$. If we choose ε and F_1 so that $b_F > 0$, then $F(t)$ is bounded above by the solution to the ODE $\dot{K}(t) = \lambda_F + \delta_{II} I_1^2 - b_F K(t)$, which is $K(t) = \frac{\lambda_F + \delta_{II} I_1^2}{b_F} + c_2 e^{-b_F t}$ for some constant c_2. This contradicts the statement that $F(t)$ grows without bound.

A.5 Stability

We have shown that if certain parameters are positive, then both I and F are finitely bounded above, and are bounded below by zero if initially they are at least zero. We also proved the existence of a unique suitable EP $E \equiv (I^{\text{ss}}, F^{\text{ss}})$. If E were unstable, then at least one of I^{ss} or F^{ss} must be unbounded. Hence E is either asymptotically stable or a stable center. The latter case is physically infeasible: the slightest perturbation in a parameter renders the stable center asymptotically stable. Moreover, because E is the unique EP and I^{ss} and F^{ss} are bounded, all trajectories tend asymptotically to E.

Fig. A4 shows a phase-plane portrait for our parameter values. Our analysis shows that any set of permissible parameters yields a phase-plane portrait exhibiting the same features. The red curve is the nullcline in Eq. (A.17) and the green curve is the nullcline in Eq. (A.18). They intersect at an equilibrium point. The blue circle indicates the equilibrium point is stable. The black curves are particular solutions.

A.6 The Special Case $\frac{\delta_{II}}{\beta_{II}} = \frac{\delta_{IF}}{\beta_{IF}}$

A closed-form solution to Eqs. (A.11)-(A.12) can be obtained by solving the cubic equation (A.16); however, this is complicated. When $\frac{\delta_{II}}{\beta_{II}} = \frac{\delta_{IF}}{\beta_{IF}} = D$, Eq. (A.15) simplifies to

$$F(I) = \frac{\lambda_F + D(\lambda_I - \mu_I I)}{\mu_F}, \tag{A.23}$$

and Eq. (A.16) reduces to the quadratic equation

$$q(I) = aI^2 + bI + c = 0, \tag{A.24}$$

where

$$\begin{aligned} a &= \mu_I D\beta_{IF} - \mu_F\beta_{II}, \\ b &= -\mu_F\mu_I - \lambda_I D\beta_{IF} - \lambda_F\beta_{IF} < 0, \\ c &= \lambda_I\mu_F. \end{aligned}$$

Note that

$$q(0) = c \geq 0, \tag{A.25}$$

$$q\left(\frac{\lambda_I}{\mu_I}\right) = -\frac{\lambda_I^2\mu_F\beta_{II}}{\mu_I^2} - \frac{\lambda_F\lambda_I\beta_{IF}}{\mu_I} \leq 0. \tag{A.26}$$

The solution to Eq. (A.24) depends upon the sign of the coefficient a. If $a = 0$, then the solution is

$$I = \frac{\lambda_I\mu_F}{\mu_I\mu_F + \lambda_I D\beta_{IF} + \lambda_F\beta_{IF}},$$

and Eq. (A.23) becomes

$$F = \frac{\lambda_F}{\mu_F} + \frac{\lambda_I D}{\mu_F}\left(\frac{\lambda_I D\beta_{IF} + \lambda_F\beta_{IF}}{\mu_I\mu_F + \lambda_I D\beta_{IF} + \lambda_F\beta_{IF}}\right). \tag{A.27}$$

If $a > 0$, then $q(I) \to \infty$ as $I \to \pm\infty$. Inequalities (A.25)-(A.26) imply that one solution is at least, and the other no more than, $\frac{\lambda_I}{\mu_I}$. The inequalities $a > 0$, $b < 0$, and $c \geq 0$ in the quadratic formula imply that all solutions are nonnegative. Hence one solution is in $\mathcal{I}$ and is given by

$$I = \frac{1}{2(\mu_I D\beta_{IF} - \mu_F\beta_{II})}\Big(\mu_F\mu_I + \lambda_I D\beta_{IF} + \lambda_F\beta_{IF} - \sqrt{(\mu_F\mu_I + \lambda_I D\beta_{IF} + \lambda_F\beta_{IF})^2 - 4\lambda_I\mu_F(\mu_I D\beta_{IF} - \mu_F\beta_{II})}\Big)$$

Finally, if $a < 0$, then $q(I) \to -\infty$ as $I \to \pm\infty$. Hence there are one or two solutions to Eqs. (A.24) and one is at least, and the other no more than, zero. Inequalities (A.25)-(A.26) show that all solutions are no greater than $\frac{\lambda_I}{\mu_I}$, and therefore one solution is in $\mathcal{I}$. That $a < 0$, $b < 0$, and $c \geq 0$ imply that the equation for I has the same form as Eq. (A.28).

B Parameter Estimation

We obtain values for the parameters in Eqs. (1)-(5). The values for the collision rate parameters $\beta_{\alpha\gamma}$, the fragment generation parameters $\delta^{\tau\kappa}_{\alpha\gamma}$, and the decay rates μ_α are found by physical modeling (Alberty & Silbey, 1997; King-Hele, 1964) and calculations using the empirical probability distributions and formulas describing satellite fragmentation and fragment characteristics developed in Johnson et al. (2001); Kessler (2000); Rossi et al. (1994). The computational framework for incorporating the data in Johnson et al. (2001) is described in §B.1. We estimate the collision rate parameters in §B.2, the fragment generation parameters in §B.3, the decay rates in §B.4, the insertion rates λ_o and λ_R in §B.5, and the initial conditions in §B.6.

B.1 Computational Framework

We take a rather lengthy detour in this subsection. Calculations for the collision rates, fragment generation rates and decay rates in §B.2-B.4 require integrating over five probability distributions, which are listed in the next paragraph, to obtain expected values. Moreover, for the collision rates and fragment generation rates, we are interested in a weighted mean where we associate two weights with a fragment. Some fragments enter highly eccentric orbits and thus spend little time at the former satellite's altitude. The first weight function, w_1, accounts for the proportion of time the fragment spends in the SOI as well as considerations related to eccentricity and deorbit time.

Fragments also vary in mass, and fragments having high mass are more hazardous to intacts than those having low mass. The second weight function, w_2, quantifies the hazard a fragment poses to an intact, and essentially defines the fragments of interest: those that are hazardous to intacts.

Of the five random variables that we consider, the empirical probability distributions in Johnson et al. (2001) govern three of them:

$$\lambda_c = \log_{10} L_c, \quad \text{where } L_c \text{ is the characteristic length,} \tag{B.1}$$
$$\chi = \log_{10}(\mathrm{A/M}), \quad \text{where A/M is the area-to-mass ratio,} \tag{B.2}$$
$$\nu = \log_{10} |\Delta v|, \quad \text{where } \Delta v \text{ is the change in velocity.} \tag{B.3}$$

These distributions depend on whether the fragment ejection event is a collision or an explosion and whether the original intact is a rocket body or a spacecraft. We are interested only in collisions. We introduce two additional random variables:

$$u, \text{ the altitude of the satellite in circular orbit generating the fragments,} \tag{B.4}$$
$$z, \text{ the direction of } \Delta v \text{ on the sphere.} \tag{B.5}$$

We use the same symbol for both a random variable and a value drawn from its distribution if the distinction is clear from the context. The random variable L_c has a power law distribution, χ is conditioned on λ_c and is a mixture of two Gaussians, ν is conditioned on χ and has a normal distribution, u is independent and uniformly distributed on the interval $[900, 1000]$ km, and z is independent and uniformly distributed on the sphere. The random vector Ω has as elements the five random variables in Eqs. (B.1)-(B.5).

Later in this section, we also use Eq. (9) from Johnson et al. (2001), which states that the average area of a fragment having characteristic length L_c is

$$A = \alpha L_c^{2+\varepsilon}, \tag{B.6}$$

where $\alpha = 0.556945$ and $\varepsilon = 0.0047077$. Rather than view A as a conditional expectation given a value of L_c, we treat Eq. (B.6) as a deterministic mapping from the realization of a random characteristic length L_c to a realization of a random area A. Similarly, a fragment that is randomly assigned the value χ from Eq. (B.2) has a random mass m given by

$$m = \frac{A}{10^{\chi}}, \tag{B.7}$$

where A is the area in Eq. (B.6). That is, a fragment's mass is determined by its characteristic length and its A/M ratio via Eqs. (B.1)-(B.2), (B.6)-(B.7).

The remainder of this subsection is organized as follows. The proportion of time a fragment spends in the SOI is calculated in §B.1.1 and the probability a collision is catastrophic is given in §B.1.2; these two calculations form the basis of our weights w_1 and w_2, respectively. Finally, the expectation of a generic function of the random vector Ω is given in §B.1.3.

B.1.1 The Fraction of Time Spent in the SOI

This subsubsection summarizes the orbital mechanics (using the equations and notation in chapter 3 of King-Hele (1964)) required to compute the fraction of time a fragment (whose properties have been sampled via Eqs. (B.1)-(B.5)) spends in the SOI; each intact in our model is assumed to be in a circular orbit. We center a polar coordinate system having unit vectors $(\hat{r}, \hat{\theta})$ at the center of the earth. Let a satellite in a circular orbit have altitude r and angle θ. A satellite sweeps out an area of an ellipse at constant rate

$$r^2\dot{\theta} = h \quad \text{(King-Hele, 1964, Eq. 3.3)}, \tag{B.8}$$

where the constant h is unique to an orbit. A satellite having velocity $v = |v|(\sin\psi\ \hat{r} + \cos\psi\ \hat{\theta})$ subtends an angle θ at rate $\dot{\theta} = \frac{|v|\cos\psi}{r}$, and so Eq. (B.8) implies that

$$h = r|v|\cos\psi. \tag{B.9}$$

The magnitude of the velocity v is related to the altitude r, gravitational parameter μ_g, and semimajor axis a by

$$v^2 = \mu_g\left(\frac{2}{r} - \frac{1}{a}\right) \quad \text{(King-Hele, 1964, Eq. 3.17)}. \tag{B.10}$$

Eccentricity e is related to the previous quantities by

$$a(1-e^2) = \frac{h^2}{\mu_g} \quad \text{(King-Hele, 1964, Eq. 3.10)}. \tag{B.11}$$

Finally, the satellite's perigee and apogee are

$$r_p = (1-e)a \quad \text{and} \quad r_a = (1+e)a. \tag{B.12}$$

Consider a satellite that is originally in a circular orbit with altitude (and therefore semimajor axis) r and velocity $v = |v|\ \hat{\theta}$, and suppose its velocity is perturbed by $\Delta v = |\Delta v|(\sin\psi\ \hat{r} + \cos\psi\ \hat{\theta})$ to $v + \Delta v$. (A perturbation orthogonal to $\hat{r}$ and $\hat{\theta}$ effectively changes the satellite's initial velocity's $\hat{\theta}$ component and so is not included here.) By Eqs. (B.9), (B.10), and (B.11) respectively, we have

$$h = r(|v| + |\Delta v| \cos\psi), \tag{B.13}$$

$$a = \frac{r\mu_g}{2\mu_g - (v + \Delta v)^2 r}, \tag{B.14}$$

$$e = \sqrt{1 - \frac{h^2}{\mu_g a}}, \tag{B.15}$$

and Eq. (B.12) gives the new apogee and perigee p.

To obtain t_p, we integrate the differential equations of motion,

$$\ddot{r} = \frac{-\mu_g}{r^2} + r\dot{\theta}^2, \tag{B.16}$$

$$\ddot{\theta} = -\frac{2\dot{r}\dot{\theta}}{r}, \tag{B.17}$$

which result from writing $F = ma$ in the $(\hat{r}, \hat{\theta})$ system, for the time duration of the orbital period, which is $2\pi\sqrt{\frac{a^3}{\mu_g}}$ by Eq. (3.20) in King-Hele (1964). We use the initial condition that the satellite is at its apogee and so initially $r = (1 + e)a$, $\dot{r} = 0$, $\theta = 0$ (arbitrarily), and $\dot{\theta} = \frac{v}{r}$, where v is obtained from Eq. (B.10). Then we compute the sum of the time intervals in which the satellite is in the SOI. This divided by $2\pi\sqrt{\frac{a^3}{\mu_g}}$ is t_p.

Each fragment is given the weight $w_1 = t_p$, which varies according to the fragment's properties in Eqs. (B.1)-(B.5). Although we assume all intacts in our model have circular orbits, we also use this calculation of t_p to help determine the launch rate in §B.5 and the initial number of intacts in §B.6.

As an aside, we conclude this subsubsection by performing a calculation (similar to one in Rossi (2002)) that is required in §4: to determine the change in velocity necessary to deorbit an intact from the SOI. We assume the intact has an area-to-mass ratio of 0.01 m^2/kg (Kaula, 1983) and does not deploy an end-of-life sail-like device to increase this ratio. The intact is initially in a circular orbit at 950 km, and by Eq. (B.10), its initial velocity is 7.375 km/s. Fig. 6-2 of NASA Safety Standard 1740.14 (1995) gives orbits as (perigee, apogee) pairs for various area-to-mass ratios that decay naturally in 25 years. We shall be interested in two pairs: $(500, 950)$ and $(510, 900)$.

We first consider the method that simply lowers the perigee to 500 km. Eqs. (B.10) and (B.12) allow us to express the velocity at perigee and apogee as

$$v_p = \sqrt{\frac{2\mu_g r_a}{r_p(r_a + r_p)}}, \tag{B.18}$$

$$v_a = \sqrt{\frac{2\mu_g r_p}{r_a(r_a + r_p)}}. \tag{B.19}$$

By considering an apogee of 950 km and a perigee of 500 km in Eq. (B.19), we find that to achieve a perigee of 500 km, its speed at apogee must be 7.257 km/s. Hence, the required change in velocity is $\Delta v = 118$ m/s. A second method first lowers the perigee to 510 km and then lowers the apogee to 900 km, and requires $\Delta v = 128$ m/s. The first method lets the spacecraft linger in the SOI for a little while; the second method shows that only 10.8% more fuel lets the spacecraft leave the SOI essentially immediately. Our model – by assuming all S_d are operational and without providing a nonoperational deorbit state – implicitly assumes the second method is used, although our estimate in the main text of the deorbit cost as a function of Δv is too crude to distinguish between the two methods.

B.1.2 The Probability a Collision is Catastrophic

In the model in Johnson et al. (2001), whether a collision is catastrophic depends on the relative velocity and masses of the objects. Because we assume that rocket bodies and spacecraft have the same mass, a particular projectile is hazardous to these two satellites with equal probability.

Fig. 9 of Johnson et al. (2001) presents, for altitudes of 200, 500, 1000, and 1500 km, a piecewise-linear probability density function $f_{v_c}(v_c)$ of the relative velocity of two objects given that they collide (i.e., the *relative collision velocity*). We use the distribution for the altitude 1000 km, and hence the result is slightly conservative relative to what we would obtain using a distribution for the altitude 950 km, which is the center of our SOI. This distribution implies that

$$\bar{v}_c \equiv E[v_c] \approx 12.1 \text{ km/s}, \tag{B.20}$$

which we shall need later.

Let two colliding objects have masses m_1 and $m_2 \geq m_1$ (in kg), and let the relative collision velocity be v_c in km/s. According to Johnson et al. (2001), the collision is catastrophic if the kinetic energy of the projectile in Joules is 40 times greater than the mass of the target in grams:

$$40 \times 10^{-3} \frac{\text{J}}{\text{g}} \leq \frac{\frac{1}{2} m_1 v_c^2}{m_2}. \tag{B.21}$$

Hence, there is a critical velocity

$$v_{\text{crit}}(m_1, m_2) = \sqrt{\frac{(80 \times 10^{-3})m_2}{m_1}}$$

such that $v_c \geq v_{\text{crit}}$ results in a catastrophic collision. Then the probability the collision is catastrophic is

$$p_c(m_1, m_2) = \int_{v_{\text{crit}}(m_1,m_2)}^{\infty} f_{v_c}(v)\ \mathrm{d}v. \tag{B.22}$$

A fragment's w_2 weight is the probability that an intact-fragment collision involving the given fragment will be catastrophic. Kessler (2000) assumes that any combination of two intacts have mass 1600 kg, and we assume that every intact has a mass of $\hat{M} = 800$ kg. In our simulation model, each fragment is assigned a random mass via Eq. (B.7). A hazardous fragment (F_τ^h) with mass m has weight $w_2 = p_c(m, \hat{M})$, and a benign fragment (F_τ^b) with mass m has weight $w_2 = 1 - p_c(m, \hat{M})$, where $p_c(m, \hat{M})$ is derived from Eq. (B.22). In §B.2, we also use Eq. (B.22) to calculate the fractions of intact-intact and fragment-fragment collisions that are catastrophic.

B.1.3 Computing Expectations

Because w_1 depends on the fragment's orbit, it is a function of ν, u, and z in Eqs. (B.3)-(B.5). Moreover, ν is conditioned on χ, and χ is conditioned on λ_c. Hence, any expectation involving the weighting function w_1 must integrate over all five probability density functions (PDFs). The weight w_2 is a function of the mass m and the hazard type $\kappa \in \{h, b\}$; we write $w_2(\cdot; \kappa)$ to indicate the latter dependence. The mass m is a function of the area A and χ via Eq. (B.7), and A is a function of λ_c by Eq. (B.1). Additionally, the PDFs of some of the random variables are parameterized by the source of the fragments (i.e., rocket bodies or spacecraft).

Let $f_\Omega(\omega; \tau, \kappa)$ be the PDF of the random vector Ω parameterized by the source $\tau \in U^I$ and the hazard type $\kappa \in \{h, b\}$, and define the weights

$$w(\omega; \kappa) \equiv \frac{w_1(\omega)w_2(\omega; \kappa)}{\int w_1(\omega)w_2(\omega; \kappa)\ d\omega}.$$

Consider first a generic function $g(\omega)$. The weighted expected value of g is

$$\mathrm{E}_w[g; \tau, \kappa] \equiv \int g(\omega) f_\Omega(\omega; \tau, \kappa) w(\omega; \kappa)\ \mathrm{d}\omega. \tag{B.23}$$

Similarly, consider a generic function $h(\omega_1, \omega_2)$, a function of two vectors independently drawn from the distribution f_Ω. The weighted expected value of h is

$$\mathrm{E}_{ww}[h;\tau_1,\kappa_1,\tau_2,\kappa_2] \equiv$$
$$\int h(\omega_1,\omega_2) f_\Omega(\omega_1;\tau_1,\kappa_1) f_\Omega(\omega_2;\tau_2,\kappa_2) w(\omega_1;\kappa_1) w(\omega_2;\kappa_2)\ \mathrm{d}\omega_1\ \mathrm{d}\omega_2. \quad \text{(B.24)}$$

In §B.2-B.4, we compute the collision rates, the fragment generation rates and the decay rates by substituting specific functions for $g(\omega)$ and $h(\omega_1, \omega_2)$ using Eqs. (B.23)-(B.24).

We approximate the expected values in Eqs. (B.23)-(B.24) by sampling the random vector Ω repeatedly and computing the sample weighted mean of the function at each sample point. We have the marginal distribution for λ_c and conditional distributions for χ and ν. Therefore, to sample Ω, we sample λ_c, then $\chi|\lambda_c$, and finally $\nu|\chi$, where '|' denotes conditioning. The random variables u and z are sampled independently.

To estimate $\mathrm{E}_w[g;\tau,\kappa]$, we start with 1 million samples. However, the distributions in Johnson et al. (2001) allow for unphysical samples. For some expectation estimates, unphysical samples can significantly alter the results. Therefore, we discard any sample whose mass exceeds the mass of an intact. In our data generation run, we discarded 642, or 0.0642%, of the samples. Let the number of samples remaining be n. To estimate $\mathrm{E}_{ww}[h;\tau_1,\kappa_1,\tau_2,\kappa_2]$, we choose, with replacement, $30n$ pairs from the n samples.

B.2 Collision Rate Parameters

We derive an analytical expression for the collision rate parameter β in §B.2.1, estimate the parameter values in this analytical expression in §B.2.2, and incorporate nonuniform spatial density in the SOI in §B.2.3.

B.2.1 Collisions Between Spherical Objects

We assume satellite collisions can be modeled by the ideal-gas model in chemical kinetics (Alberty & Silbey, 1997). Consider two spheres contained in a large volume V having radii r_1 and r_2, cross sections $\sigma_i = \pi r_i^2$, and relative speed $v_{12}(t)$. They collide if their centers are within a distance $d_{12} = r_1 + r_2$, referred to as the collision diameter, of each other. We view a collision from the perspective of sphere 1 so that sphere two is moving relative to sphere 1's fixed position. In an infinitesimal time $\mathrm{d}t$, if sphere two is anywhere within a cylinder having base πd_{12}^2, which is called the collision cross section, and height $v_{12}(t)\ \mathrm{d}t$, then there is a collision. The cylinder fills a proportion $\frac{\pi d_{12}^2 v_{12}(t)\ \mathrm{d}t}{V}$ of the total volume. Given no other information – e.g., the initial position of the spheres – it is reasonable to take this proportion as the probability of these two spheres colliding in the time interval $[t, t + \mathrm{d}t]$.

Incorporating randomness, we now suppose a sphere has radius R distributed according to $f_R(r)$, and two spheres have relative speeds $v_{12} \sim f_{v_{12}}(v)$. The expected volume of the cylinder is

$$\int \pi(r_1 + r_2)^2 \; v_{12} f_R(r_1) f_R(r_2) f_{v_{12}}(v) \; \mathrm{d}r_1 \; \mathrm{d}r_2 \; \mathrm{d}v = \pi \bar{v}_{12} \int (r_1 + r_2)^2 f_R(r_1) f_R(r_2) \; \mathrm{d}r_1 \; \mathrm{d}r_2,$$

where $\bar{v}_{12} \equiv \int v_{12} f_{v_{12}}(v) \; \mathrm{d}v$ is the *collision probability velocity* (this is not the same quantity as $\bar{v}_c$: $\bar{v}_{12}$ is the average relative velocity of two objects and $\bar{v}_c$ is the average relative velocity given two objects have collided). The expected number of collisions in time $\mathrm{d}t$ between N spheres having radii $R \sim f_R(r)$ and relative speeds $v_{12} \sim f_{v_{12}}(v)$ is

$$\frac{1}{2} \frac{N^2 \pi \bar{v}_{12}}{V} \int (r_1 + r_2)^2 f_R(r_1) f_R(r_2) \; \mathrm{d}r_1 \; \mathrm{d}r_2, \tag{B.25}$$

where the factor $\frac{1}{2}$ avoids double counting spheres. Hence, by Eqs. (1)-(5), the parameter β corresponds to $\frac{\pi \bar{v}_{12}}{V} \int (r_1 + r_2)^2 f_R(r_1) f_R(r_2) \; \mathrm{d}r_1 \; \mathrm{d}r_2$, or simply $\frac{\pi \bar{v}_{12}}{V} E[d_{12}^2]$.

As in Johnson et al. (2001); Kessler (2000), we estimate β using the collision cross section σ_{12} rather than the collision diameter d_{12}. If all objects are assumed to be spherical, then these two quantities are related via $\sigma_{12} = \pi d_{12}^2$, and hence the collision cross section can be expressed in terms of the individual cross sections by $\sqrt{\sigma_{12}} = \sqrt{\sigma_1} + \sqrt{\sigma_2}$. Therefore, we can write β as $\frac{\bar{v}_{12}}{V} E[\sigma_{12}]$.

Finally, while the w_2 weights in §B.1.2 quantify the fraction of intact-fragment collisions that are catastrophic, we have yet to account for the fraction of intact-intact and fragment-fragment collisions that are catastrophic. We do so using the variable ψ, where a proportion $1 - \psi$ of collisions are disregarded because they are not catastrophic; as shown in §B.2.2, ψ is derived for various intact-intact and fragment-fragment collisions using the probabilites $p_c(m_1, m_2)$ in Eq. (B.22). Hence, we define the collision rate parameter by

$$\tilde{\beta} \equiv \frac{\bar{v}_{12}}{V} E[\psi \sigma_{12}], \tag{B.26}$$

where the tilde denotes that the spatial density of satellites is assumed to be uniform in the SOI. In §B.2.3, we multiply $\tilde{\beta}$ by a nonuniformity factor to obtain the collision rate parameter β.

B.2.2 Estimating Parameters in Eq. (B.26)

In this subsubsection, we estimate the quantities V, $\bar{v}_{12}$, σ_{12}, and ψ in Eq. (B.26). The earth's radius is 6378 km, and hence the volume of our compartment is $V = \frac{4}{3}\pi\left((6378+1000)^3 - (6378+900)^3\right) = 6.748 \times 10^{10}$ km^3. We take the collision probability velocity to be $\bar{v}_{12}$ =8.8 km/sec (Johnson et al., 2001, Fig. 8).

For $\alpha, \gamma \in \{U\}$, we have $\sqrt{\sigma_{\alpha\gamma}} = \sqrt{\sigma_\alpha} + \sqrt{\sigma_\gamma}$, and it remains to determine σ_S, σ_R, and $\sigma_{F_\tau^\kappa}$. In his calculations, Kessler (Kessler, 2000) assumes that the collision cross section of a fragment is zero; hence his cross section values are for intacts only. We do not know the individual cross sections of spacecraft or rocket bodies and so must use average values to obtain σ_S and σ_R. Kessler obtains average cross sections for the region [920,1020] km of $\sigma_f = 14.1$ m^2 for intact-fragment collisions and $\sigma_i = 53.8$ m^2 for intact-intact collisions (Kessler, 2000). The ratio $\sigma_i/\sigma_f = 3.82 < 4$ (by less than 5%) because σ_i is computed by averaging over all intact-intact combinations in his database. Our calculations assume the ratio is exactly 4, effectively using only the 14.1 m^2 value. Kessler observes that spacecraft have an average cross section 0.35 times the average, or $\sigma_S = 0.35 \times 14.1 = 4.94$ m^2, and rocket bodies have an average cross section $\sigma_R = 1.65 \times 14.1 = 23.3$ m^2 (Kessler, 2000).

For fragments we have a probability distribution over the area A from Eq. (B.6), which corresponds to the cross section under the assumption that fragments are spherical. Under this assumption, the collision cross section for an intact and fragment is

$$\sigma_{\alpha F_\tau^\kappa} = \left(\sqrt{\sigma_\alpha} + \sqrt{A}\right)^2, \tag{B.27}$$

and the collision cross section for two fragments is

$$\sigma_{F_{\tau_1}^{\kappa_1} F_{\tau_2}^{\kappa_2}} = \left(\sqrt{A_1} + \sqrt{A_2}\right)^2. \tag{B.28}$$

The final parameters to estimate are the catastrophic probabilities ψ. The change over time of the proportion of fragments that are hazardous to intacts is accounted for by the separate hazardous and benign fragment types and corresponding equations in Eqs. (1)-(5) and the w_2 weights in §B.1.2. Therefore, all intact-fragment collisions are counted and we set $\psi_{\alpha F_\tau^\kappa} = 1$ for $\alpha \in U^I$.

All intacts have the same mass, $\hat{M} = 800$ kg. Therefore, each poses the same threat to the others, and Eq. (B.22) implies that

$$\psi_I \equiv \psi_{\alpha\gamma} = p_c(\hat{M}, \hat{M}) = 0.9996 \quad \text{for} \quad \alpha, \gamma \in U^I; \tag{B.29}$$

i.e., nearly all intact-intact collisions are catastrophic.

Fragments pose different hazards to each other. By Eq. (B.22), the probability that a collision between a fragment of type $F_{\tau_1}^{\kappa_1}$ with mass m_1 and one of type $F_{\tau_2}^{\kappa_2}$ with mass m_2 is catastrophic is

$$\psi_{F_{\tau_1}^{\kappa_1} F_{\tau_2}^{\kappa_2}} = p_c(m_1, m_2). \tag{B.30}$$

For all types of fragment-fragment collisions, $\psi > 0.96$ when averaged over Ω.

Though Johnson et al. (2001) defines a non-catastrophic collision as one in which only the less massive object breaks up, we assume that in intact-intact and fragment-fragment collisions, a non-catastrophic collision produces no new fragments. Because essentially all intact-intact and almost all fragment-fragment collisions are catastrophic, there is little error in making this assumption, and the error is conservative. As in Johnson et al. (2001), we assume that only the less massive object breaks up in non-catastrophic intact-fragment collisions.

We have put more work into modeling intact-fragment than intact-intact and intact-fragment collisions. However, the intact-intact collisions are modeled accurately simply because such a collision is nearly always catastrophic. The fragment-fragment collisions have a static parameter ψ, which is inaccurate if the properties of the fragment population change over time (which must happen in the presence of fragment-fragment collisions). However, we investigate this issue by comparing two versions of Eqs. (1)-(5): one with, and one without, fragment-fragment collisions.

The value of $\tilde{\beta}$ is obtained by taking the expectation in Eq. (B.26) and substituting Eqs. (B.27)-(B.30) for the generic functions in Eqs. (B.23)-(B.24). For intact-intact collisions, Eq. (B.26) contains no random variables and we have

$$\tilde{\beta}_{\alpha\gamma} = \frac{\bar{v}_{12}}{V} \psi_I \sigma_{\alpha\gamma} \quad \text{for} \quad \alpha, \gamma \in U^I, \tag{B.31}$$

where ψ_I is given in Eq. (B.29). For intact-fragment collisions, we have

$$\tilde{\beta}_{\alpha F_\tau^\kappa} = \frac{\bar{v}_{12}}{V} \mathrm{E}_w[\sigma_{\alpha F_\tau^\kappa}; \tau, \kappa], \tag{B.32}$$

and for fragment-fragment collisions, we have

$$\tilde{\beta}_{F_{\tau_1}^{\kappa_1} F_{\tau_2}^{\kappa_2}} = \frac{\bar{v}_{12}}{V} \mathrm{E}_{ww}[\psi_{F_{\tau_1}^{\kappa_1} F_{\tau_2}^{\kappa_2}} \sigma_{F_{\tau_1}^{\kappa_1} F_{\tau_2}^{\kappa_2}}; \tau_1, \kappa_1, \tau_2, \kappa_2]. \tag{B.33}$$

The numerical values from Eqs. (B.31)-(B.33) for both versions of the model (i.e., in the absence and presence of fragment-fragment collisions) appear in Tables B.1-B.2. The rows and columns of the matrices correspond to the left and right subscripts, respectively, of $\tilde{\beta}_{\alpha\gamma}$ and $\frac{\delta_{\alpha\gamma}^{\tau\kappa}}{\tilde{\beta}_{\alpha\gamma}}$. All time units are in years.

B.2.3 Nonuniform Spatial Density

Satellites are distributed nonuniformly throughout the SOI for two reasons: a satellite having an approximately circular orbit tends to spend a greater proportion of time at latitudes near its inclination than at other latitudes, and the volume of the SOI as a function of latitude decreases near the poles. We incorporate this these phenomena into our model by considering a nonuniform version of the ideal gas model.

Consider populations of two types of spherical objects mixed homogeneously in a region of space having volume V. Each population has number density $\rho_i \equiv \frac{n_i}{V}$, $i = 1, 2$. The ideal gas model gives the number of collisions c in a unit of time as

$$c = b_{12} V \rho_1 \rho_2 = b_{12} \frac{n_1 n_2}{V} \tag{B.34}$$

for some constant b_{12}.

Suppose the objects prefer some parts of space over others. Break the region into voxels v_j, each having volume V_j. Let the objects of type i have number density $n_i \rho_{ij}$; that is, if one measured the locations of the objects for a long time, one would find their locations distributed according to the density ρ_{ij}. Because $\sum_j V_j n_i \rho_{ij} = n_i$ by definition, we have $\sum_j V_j \rho_{ij} = 1$, and so ρ_{ij} is indeed a density function. Eq. (B.34) holds in each voxel v_j; summing over the voxels yields

$$\begin{aligned} c &= b_{12} n_1 n_2 \sum_j V_j \rho_{1j} \rho_{2j} \\ &= f_{12} b_{12} \frac{n_1 n_2}{V}, \end{aligned}$$

where we define

$$f_{12} \equiv V \sum_j V_j \rho_{1j} \rho_{2j} \tag{B.35}$$

to be the nonuniformity factor.

If the density is uniform then $n_i \rho_{ij} = \frac{n_i}{V}$ and

$$\begin{aligned} c &= \left(V \sum_j V_j \rho_{1j} \rho_{2j} \right) b_{12} \frac{n_1 n_2}{V} \\ &= b_{12} \sum_j V_j \frac{n_1}{V} \frac{n_2}{V} \\ &= b_{12} \frac{n_1}{V} \frac{n_2}{V} \sum_j V_j \\ &= b_{12} \frac{n_1 n_2}{V}, \end{aligned}$$

and hence $f_{12} = 1$.

If the density ρ_{ij} changes with time, then f_{12} also changes with time. But suppose the density ρ_{ij} is constant in time and so only the numbers n_i change. Then f_{12} is constant, and

$$c(t) = f_{12} b_{12} \frac{n_1(t) n_2(t)}{V} \quad \text{for all} \quad t \geq 0.$$

Hence, we can accommodate spatial nonuniformity in our ODE model by simply multiplying the rate $\tilde{\beta}$ by the nonuniformity factor. More specifically, in the remainder of this section we calculate $f_{\alpha\gamma}$ for $\alpha, \gamma \in \{R, S, F\}$, which allows us to use Eqs. (B.31)-(B.33) to define the collision rate parameters

$$\beta_{\alpha\gamma} = f_{\alpha\gamma} \tilde{\beta}_{\alpha\gamma} \quad \text{for} \quad \alpha, \gamma \in U^I, \tag{B.36}$$

$$\beta_{\alpha F_\tau^\kappa} = f_{\alpha F} \tilde{\beta}_{\alpha F_\tau^\kappa} \quad \text{for} \quad \alpha \in U^I, \tag{B.37}$$

$$\beta_{F_{\tau_1}^{\kappa_1} F_{\tau_2}^{\kappa_2}} = f_{FF} \tilde{\beta}_{F_{\tau_1}^{\kappa_1} F_{\tau_2}^{\kappa_2}}. \tag{B.38}$$

To determine the density of satellites at a particular latitude, we use the current publicly available catalog (Space Track, 2008) and build a histogram for each of our three classes of satellites—fragments, rocket bodies, and spacecraft. Because the density is empirical, we must compute it by discretizing the SOI. We create 90 voxels, where voxel v_j, $j \in 1, 2, \ldots, 90$, spans the latitudes $(j-1)^\circ$ to j° and the altitudes of the SOI, $R_e + 900$ km to $R_e + 1000$ km. To compute a density, we need two pieces of information: the volume V_j of voxel v_j and the expected number of satellites in the voxel.

Using spherical coordinates, the volume of voxel v_j is

$$V_j = \int_{\frac{\pi}{2} + \frac{(j-1)\pi}{180}}^{\frac{\pi}{2} + \frac{j\pi}{180}} \int_{R_e+900}^{R_e+1000} \int_0^{2\pi} r^2 \sin\phi \, \mathrm{d}\theta \, \mathrm{d}r \, \mathrm{d}\phi.$$

Now consider the orbit of a particular satellite. We must calculate the latitude and altitude of the satellite as a function of time: $(l(t), r(t))$. Four Keplerian orbital elements are relevant: the apogee a, the eccentricity e, the inclination i, and the argument of periapsis ω. We use the procedure described at the end of §B.1.1 to compute $(\hat{\theta}(t), r(t))$, the position of the satellite in its orbital plane, in polar coordinates, as a function of time.

Recall from Eqs. (B.16)-(B.17) that we integrate the equations of motion for one orbit, starting at apogee. Therefore, $\hat{\theta} = 0$ when the satellite is at apogee. To calculate l from $\hat{\theta}$, we must translate $\hat{\theta}$ to an angle θ such that $\theta \mod 2\pi = 0$ at the time the satellite crosses the equator. Because ω is the angle in the orbital plane between the equator and the satellite at perigee, and the apogee and perigee are opposite each other, it follows that $\theta \equiv \hat{\theta} + \pi + \omega$.

The vertical distance of the satellite above the plane of the equator is $r \sin l$. We derive another expression for the vertical distance using θ and i and equate the two expressions. The distance, in the orbital plane, of the satellite above the equator is $r \sin \theta$. Multiplying this distance by $\sin i$ gives the satellite's vertical distance above the plane of the equator. Hence $r \sin l = r \sin \theta \sin i$ and so $l = \sin^{-1}(\sin \theta \sin i)$.

Next, we use $(l(t), r(t))$ for one orbit to calculate the proportion of time the satellite spends in the SOI in each latitude bin, which allows us to produce histograms for the three satellite categories (Fig. B1). The histograms of the expected number of satellites per latitude bin (Fig. B1a) increase near the poles because of the first reason cited at the beginning of this subsubsection. Dividing the number of satellites in each latitude bin by the volume of the corresponding voxel and normalizing the results produces densities $\rho_{\alpha j}$ for $\alpha \in \{R, S, F\}$ that increase near the poles (Fig. B1b) because of both reasons cited at the beginning of this subsubsection.

The nonuniformity factors $f_{\alpha\gamma}$ are calculated via Eq. (B.35) and appear in Table B.3. Fig. B1 and subsequent analysis of the catalog shows that there are a large number of SL-8 rocket bodies having inclinations between 82° and 83°; their presence is the primary reason why $f_{R\gamma}$ is larger than the other nonuniformity factors.

B.3 Debris Generation Parameters

Using Eq. (B.25) as a starting point, we derive an expression for the debris generation parameter. Suppose that in addition to a radius R, a sphere has a mass M, and that the random variables $(R, M) \equiv \tilde{\Omega} \sim f_{\tilde{\Omega}}(\tilde{\omega})$. Colliding spheres break up to produce fragments. A collision between spheres 1 and 2 generates $\hat{N}(m_1, m_2)$ fragments. Then the expected number of fragments generated per unit time is

$$\frac{1}{2} \frac{N^2 \pi \bar{v}_{12}}{V} \int \hat{N}(m_1, m_2)(r_1 + r_2)^2 f_{\tilde{\Omega}}(\tilde{\omega}_1) f_{\tilde{\Omega}}(\tilde{\omega}_2) \, \mathrm{d}\tilde{\omega}_1 \, \mathrm{d}\tilde{\omega}_2.$$

Recalling that $d_{12} = r_1 + r_2$ and $\sigma_{12} = \pi d_{12}^2$, by Eqs. (1)-(5), we see that the debris generation parameter δ corresponds to

$$\frac{\bar{v}_{12}}{V} \int \hat{N}(m_1, m_2) \sigma_{12} f_{\tilde{\Omega}}(\tilde{\omega}_1) f_{\tilde{\Omega}}(\tilde{\omega}_2) \, \mathrm{d}\tilde{\omega}_1 \, \mathrm{d}\tilde{\omega}_2, \tag{B.39}$$

except that Eq. (B.39) does not take into account the variable ψ (see Eq. (B.26)) and the fact that a fragment's orbit is often only partly in the SOI after a fragmentation event. The expected proportion of time that a fragment—of type F_τ^κ and produced by an intact of type $\alpha \in U^I$ or a fragment

of type F_α^h in a catastrophic collision—spends in the SOI is

$$s_\alpha^{\tau\kappa} = \begin{cases} 0 & \text{if } \tau \neq \alpha; \\ \int w_1(\omega) w_2(\omega;\kappa) f_\Omega(\omega;\tau,\kappa)\ \mathrm{d}\omega & \text{if } \tau = \alpha. \end{cases} \tag{B.40}$$

The integral in Eq. (B.40) is the expectation of the product of the weights w_1 and w_2 defined in §B.1.1-B.1.2. A benign fragment of type F_α^b generates only benign fragments and so w_2 is excluded:

$$s_\alpha^{\tau b} = \begin{cases} 0 & \text{if } \tau \neq \alpha; \\ \int w_1(\omega) f_\Omega(\omega;\tau,b)\ d\omega & \text{if } \tau = \alpha. \end{cases}$$

These expectations are independent of what follows because they concern a property of the proportion of fragments generated, which, except for intact source type, is independent of properties of the colliding fragments.

We now define the function $D_{\alpha\gamma}^{\tau\kappa}$, which quantifies – for specific fragment property values – the number of fragments emerging from a collision weighted by the fraction of time $s_\alpha^{\tau\kappa}$ in Eqs. (B.40)-(B.41) that fragments spend in the SOI. Then, by Eq. (B.39), we have

$$\delta_{\alpha\gamma}^{\tau\kappa} = \frac{\bar{v}_{12}}{V} E[D_{\alpha\gamma}^{\tau\kappa} \psi_{\alpha\gamma} \sigma_{\alpha\gamma}]. \tag{B.41}$$

We need the specific power law distribution given in Eq. (4) in Johnson et al. (2001), which states that the number of fragments from a collision having characteristic length at least L_c meters is

$$N(L_c; M) = 0.1 M^{0.75} L_c^{-1.71}, \tag{B.42}$$

where M is the mass of the objects involved if the collision is catastrophic, and M is the product of the mass of the less massive object and the relative collision velocity v_c in a non-catastrophic collision. We are interested only in fragments having $L_c \geq \hat{L}_c \equiv 10$ cm, and for convenience we define $\hat{N}(M) \equiv N(\hat{L}_c; M)$.

Consider a catastrophic collision between two objects of masses m_i, $i = 1, 2$. The collision produces $\hat{N}(m_1 + m_2)$ fragments. We assume – this assumption goes beyond the model in Johnson et al. (2001) – that the proportion of fragments object i generates is $\frac{m_i}{m_1+m_2}$, $i = 1, 2$. Each object produces fragments of various types.

We first derive $D_{\alpha\gamma}^{\tau\kappa}$ for intact-intact collisions. A collision between two intacts of types $\alpha, \gamma \in U^I$ generates

$$D_{\alpha\gamma}^{\tau\kappa} = \frac{\hat{N}(2\hat{M})(s_\alpha^{\tau\kappa} + s_\gamma^{\tau\kappa})}{2} \tag{B.43}$$

fragments of type F_τ^κ. In intact-intact collisions, $D_{\alpha\gamma}^{\tau\kappa}$ and $\beta_{\alpha\gamma}^{\tau\kappa}$ are independent.

A collision between an intact of type $\alpha \in U^I$ and a benign fragment of type F_τ^b and having mass m is non-catastrophic; only the benign fragment breaks up. The fragment generates

$$D_{\alpha F_\tau^b}^{\tau b} \equiv \hat{N}(m\bar{v}_c)s_\tau^{\tau b} - 1$$

fragments also of type F_τ^b, where we make use of $\bar{v}_c = 12.1$ km/s from Eq. (B.20). The -1 accounts for the loss of the original fragment.

A catastrophic collision between an intact of type $\alpha \in U^I$ having mass $\hat{M}$ and a fragment of type $F_{\tau_1}^h$ having mass m generates, by Eqs. (B.39)-(B.41),

$$D_{\alpha F_{\tau_1}^h}^{\tau_2\kappa} \equiv \hat{N}(\hat{M}+m)\left(\frac{\hat{M}}{\hat{M}+m}s_\alpha^{\tau_2\kappa} + \frac{m}{\hat{M}+m}s_{\tau_1}^{\tau_2\kappa}\right) - \delta(\tau_1,\tau_2)$$

fragments of type $F_{\tau_2}^{\kappa_2}$, where $\delta(\tau_1,\tau_2) = 1$ if $\tau_1 = \tau_2$ and 0 otherwise. The second term in parentheses is neglected in the fragment-fragment version of the model.

Finally, by Eq. (B.39)-(B.41), a catastrophic collision between two fragments of types $F_{\tau_1}^{\kappa_1}$ and $F_{\tau_2}^{\kappa_2}$ generates

$$D_{F_{\tau_1}^{\kappa_1}F_{\tau_2}^{\kappa_2}}^{\tau_3\kappa_3} \equiv \hat{N}(m_1+m_2)\left(\frac{m_1}{m_1+m_2}s_{F_{\tau_1}^{\kappa_1}}^{\tau_3\kappa_3} + \frac{m_2}{m_1+m_2}s_{F_{\tau_2}^{\kappa_2}}^{\tau_3\kappa_3}\right) - \delta(\tau_3,\tau_1) - \delta(\tau_3,\tau_2)$$

fragments of type $F_{\tau_3}^{\kappa_3}$.

We conclude this subsection by taking the expectation in Eq. (B.41). For an intact-intact collision, the expressions do not have any random variables, and

$$\delta_{\alpha\gamma}^{\tau\kappa} \equiv \frac{\hat{N}(2\hat{M})(s_\alpha^{\tau\kappa} + s_\gamma^{\tau\kappa})\bar{v}_{12}\psi_I\sigma_{\alpha\gamma}}{2V}. \tag{B.44}$$

For a collision between an intact and a benign fragment, we have

$$\delta_{\alpha F_\tau^b}^{\tau b} \equiv \frac{\bar{v}_{12}\mathrm{E}_w\left[D_{\alpha F_\tau^b}^{\tau b}\sigma_{\alpha F_\tau^b};\tau,b\right]}{V}, \tag{B.45}$$

and for a collision between an intact and a hazardous fragment, we have

$$\delta_{\alpha F_{\tau_1}^h}^{\tau_2\kappa} \equiv \frac{\bar{v}_{12}\mathrm{E}_w\left[D_{\alpha F_{\tau_1}^h}^{\tau_2\kappa}\sigma_{\alpha F_{\tau_1}^h};\tau_1,h\right]}{V}. \tag{B.46}$$

Finally, the expectation for a catastrophic collision between two fragments is

$$\delta_{F_{\tau_1}^{\kappa_1}F_{\tau_2}^{\kappa_2}}^{\tau_3\kappa_3} \equiv \frac{\bar{v}_{12}\mathrm{E}_{ww}\left[D_{F_{\tau_1}^{\kappa_1}F_{\tau_2}^{\kappa_2}}^{\tau_3\kappa_3}\psi_{F_{\tau_1}^{\kappa_1}F_{\tau_2}^{\kappa_2}}\sigma_{F_{\tau_1}^{\kappa_1}F_{\tau_2}^{\kappa_2}};\tau_1,\kappa_1,\tau_2,\kappa_2\right]}{V}. \tag{B.47}$$

Although Eqs. (B.44)-(B.47) yield $\delta_{\alpha\gamma}^{\tau\kappa}$, we display values for $\frac{\delta_{\alpha\gamma}^{\tau\kappa}}{\beta_{\alpha\gamma}}$, which has a more intuitive meaning as the average number of fragments of a certain type generated by a certain type of collision. These numerical values for both versions of the model appear in Tables B.1-B.2.

B.4 Decay Rates

In this subsection, we estimate the decay rates for intacts with deorbit capability (μ_o), intacts without deorbit capability (μ_R and μ_n), and fragments ($\mu_{F_\tau^\kappa}$). We set $\mu_o^{-1} = 3$ yr, which reflects the historical average of a 3-year mission lifetime and the 25-year decay rule recommended by NASA safety guidelines (NASA Safety Standard 1740.14, 1995; Liou & Johnson, 2005), in which spacecraft or upper stages are placed in an orbit that will result in a remaining lifetime of < 25 years.

We estimate the decay rates μ_R, μ_n, and $\mu_{F_\tau^\kappa}$ as reciprocals of residence times. Table 4 in Rossi et al. (1994) gives the residence time in years of a satellite in various shells, and the residence time for the SOI is 110 years. The table is calibrated for an A/M ratio of 1 m^2/kg; the residence time for a satellite having a different value of A/M is obtained by dividing the time by that value.

Recommended values for the A/M ratio for intacts range between 2×10^{-3} and 2×10^{-2} m^2/kg (Kaula, 1983), which yield residence times of between 5.5×10^3 and 5.5×10^4 years. Either of these values makes the decay rate for intacts insignificant in the next few centuries. We use $\mu_R = \mu_n = \frac{1 \times 10^{-2}}{110} = 9.1 \times 10^{-5}$/yr.

The 4 fragment types F_τ^κ have different average A/M values. By Eqs. (B.2) and (B.23), we compute the fragment decay rates via

$$\mu_{F_\tau^\kappa} = \frac{\mathrm{E}_w[10^\chi; \tau, \kappa]}{110}. \tag{B.48}$$

The numerical results from Eq. (B.48) appear in Table B.4. Kessler (2000) uses a decay rate of $\frac{1}{493}$ per year, which is between the four fragment decay rates calculated from Eq. (B.48).

B.5 Insertion Rates

In this subsection, we estimate λ_o, which is the insertion rate of new spacecraft into the SOI, and λ_R, which is the insertion rate of rocket bodies in

the SOI, by inspecting historical values. We obtained a full catalog of satellite element sets from Space Track (2008) for the date December 31, 2007 at 12:00 a.m. The catalog is an ASCII file containing a list of, in our case, 11307 two-line element sets with an additional brief text description of the satellite.

First, we filter out all entries whose text descriptions contain any of the words "DEB", "FUEL", or "COOLANT", which leaves 4431 entries. Next, we compute the effective number of spacecraft in the SOI by launch year, by computing (using §B.1.1) the proportion of time each satellite spends in the SOI. We assume rocket bodies have the word "R/B" in their text entry and spacecraft do not. The result is that there are 207.2 effective spacecraft in the SOI and 183.3 effective rocket bodies in the SOI. Fig. B3 shows the effective number of spacecraft and rocket bodies inserted into the SOI by launch year. Inspecting the insertion rates for the past decade, we set $\lambda_o = 3/\text{yr}$ and $\lambda_R = 1/\text{yr}$. As noted in the main text, we set $\lambda_R = 0$ after 10 yr, and set $\lambda_{F_\tau^\kappa} = 0$ and $\theta_d = \frac{2}{3}$.

B.6 Initial Conditions

We use the catalog described in §B.5 to determine the initial number of satellites of each type. Recall that the sensors in the U.S. Space Surveillance Network generally can resolve objects no smaller than 10 cm, our threshold for fragments. First, we find all entries marked with "DEB" and count these as fragments. Then, in the same way that we derived $R(0) = 183.3$ and $S(0) = 207.2$ in §B.5, we find that the initial effective number of fragments is $F^s(0) = 955.5$.

To determine initial conditions for our model, we must split the initial satellites into spacecraft with and without deorbit capability, and allocate the initial fragments among the 4 fragment types. We set $S_n^o(0) = \frac{(1-\theta_d)\lambda_o}{\mu_o} = 3$ and $S_d(0) = \frac{\theta_d \lambda_o}{\mu_o} = 6$, which are the equilibrium values if we ignore collisions in Eqs. (3)-(4), and set $S_n(0) = S(0) - S_n^o(0) - S_d(0) = 198.2$. In Farinella & Cordelli (1991), it is suggested that most fragments are from exploding rocket bodies. We assume 90% of the initial fragments are from rocket bodies, with one exception that is allocated entirely to a spacecraft source: by separately analyzing the fragment entries that additionally contain the tag "FENGYUN 1C", we calculate that 400.9 of the 955.5 initial effective fragments in the SOI are from the Chinese ASAT test resulting in the break up of the FengYun 1C spacecraft, which broke up at $\approx$ 850 km (Liou & Portman, 2007). Though the number 90% is just a guess, the results are insensitive to it; moreover, a smaller proportion from rocket bodies yields a higher fraction of hazardous fragments, and so choosing a high proportion is conservative. Finally, we use the parameters $s_\alpha^{\tau\kappa}$ in Eq. (B.40), i.e., the proportion of fragments of type F_τ^κ

generated by the break up of an intact α, to determine the mix of hazardous and benign fragments. This is a conservative choice because benign fragments deorbit faster than hazardous ones on average and so if no new breakups occur, the proportion of hazardous fragments increases with time. These allocations result in the initial conditions $F_S^h(0) = 169.8$, $F_R^h(0) = 106.2$, $F_S^b(0) = 286.5$, and $F_R^b(0) = 393.0$. Using the same procedure, we find that of the 400.9 fragments from the FengYun 1C spacecraft, 149.1 are hazardous and 251.8 are benign.

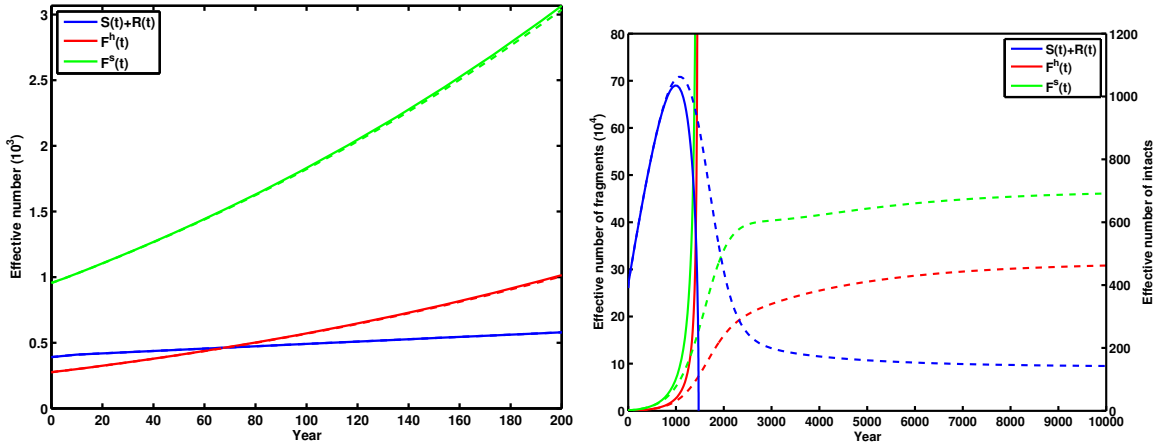

(a) (b)

Fig. B.1. **Fig. 1.** The solution to both versions of Eqs. (1)-(5) for **(a)** 200 yr and **(b)** 10^4 yr. The dashed curves ignore fragment-fragment collisions, and the solid curves include fragment-fragment collisions.

Table 1
Comparison of the fragment-fragment version of Eqs. (1)-(5) to Liou & Johnson (2008). For Liou & Johnson (2008), these are the average number of collisions (averaged over 150 Monte Carlo simulations) in the SOI for the results appearing in Fig. 8 in Liou & Johnson (2008) (private communication, Nicholas Johnson).

Object type	Number of collisions for the next 200 years		Catastrophic/ non-catastrophic	
	(1)-(5)	Liou & Johnson (2008)	(1)-(5)	Liou & Johnson (2008)
Intact-intact	4.38	2.65	4.38/0.00	2.64/0.01
Intact-fragment	6.83	6.43	2.26/4.57	2.83/3.60
Fragment-fragment	0.58	0.58	0.47/0.11	0.39/0.19
Total	11.79	9.66	7.11/4.68	5.06/3.27

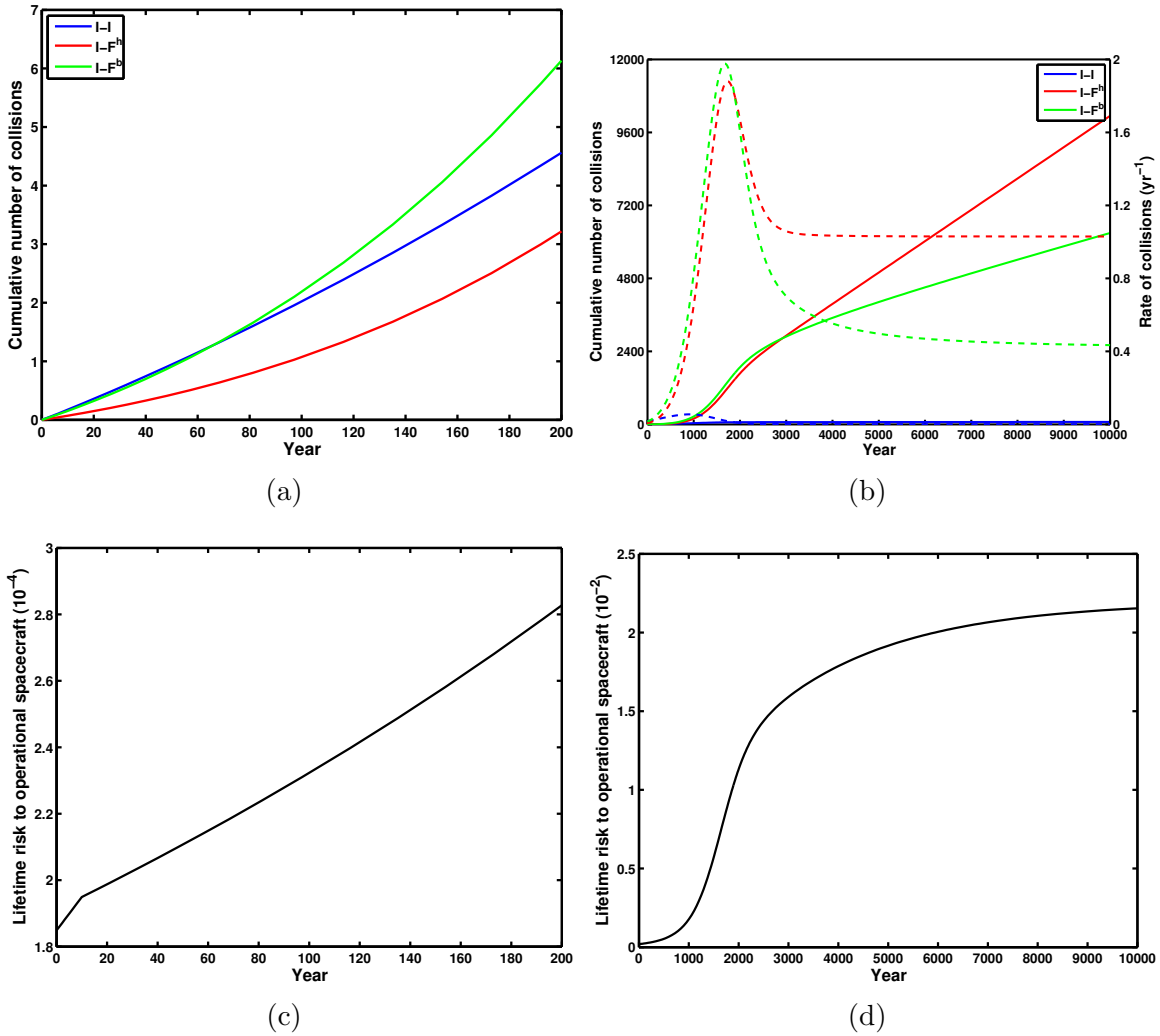

Fig. B.2. **Fig. 2. (a)** Cumulative number of intact-intact, catastrophic intact-fragment, and noncatastrophic intact-fragment collisions over the first 200 yr; **(b)** cumulative number (—) and instantaneous rate (- - -) of these collisions over 10^4 yr; and the lifetime risk to an operational spacecraft in Eq. (8) vs. time for **(c)** 200 yr and **(d)** 10^4 yr.

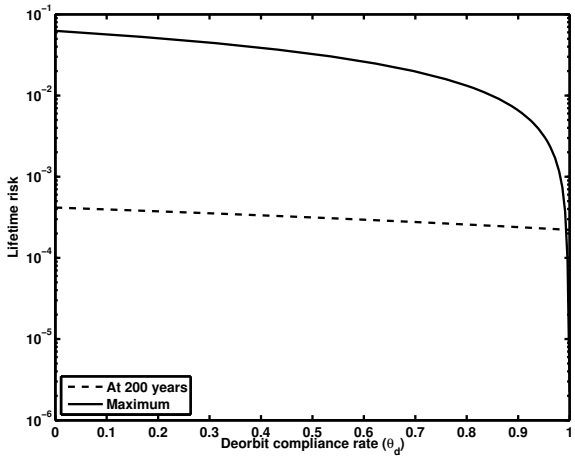

Fig. B.3. **Fig. 3.** The maximum lifetime risk to an operational spacecraft, i.e. $\max_{t\geq 0} r^o(t)$ in Eq. (8), (—) and the lifetime risk at $t = 200$ yr (- - -) vs. the proportion θ_d of new launches that deorbit the spacecraft at the end of its operational life.

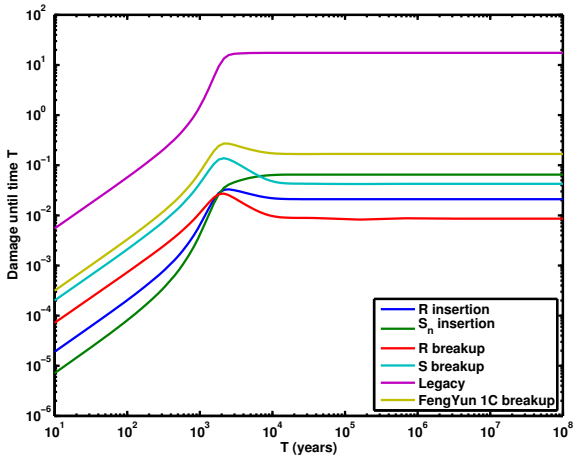

Fig. B.4. **Fig. 4.** The damage (i.e., destroyed operational spacecraft) up until time T caused by various activities that occur at time 0.

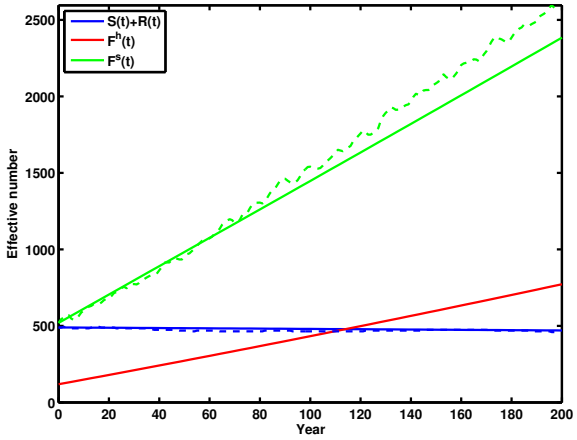

Fig. B.5. **Fig. A1.** Comparison of the fragment-fragment version of Eqs. (1)-(5) (—) to the results in Fig. 8 of Liou & Johnson (2008) (- -).

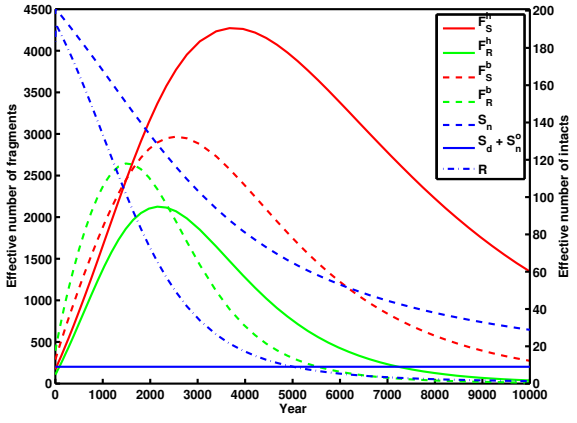

Fig. B.6. **Fig. A2.** The solution to Eqs. (1)-(5) over 10^4 yr when there is full compliance with spacecraft deorbiting ($\theta_d = 1$).

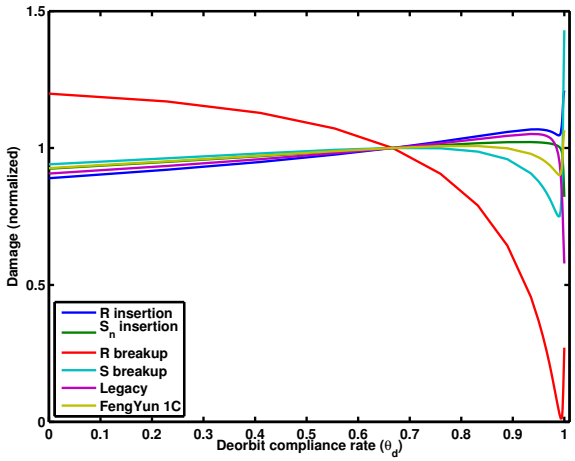

Fig. B.7. **Fig. A3.** Damage (normalized to 1 at $\theta_d = \frac{2}{3}$) for various activities vs. the deorbit compliance rate θ_d. The behavior for $\theta_d > 0.98$ appears to be due to two competing behaviors: a smaller θ_d amplifies the effects of a single event but also decreases the probability that the loss of a particular operational spacecraft will be due (directly or indirectly) to the event. The high decay rate of rocket body fragments causes the former effect to dominate for this satellite type.

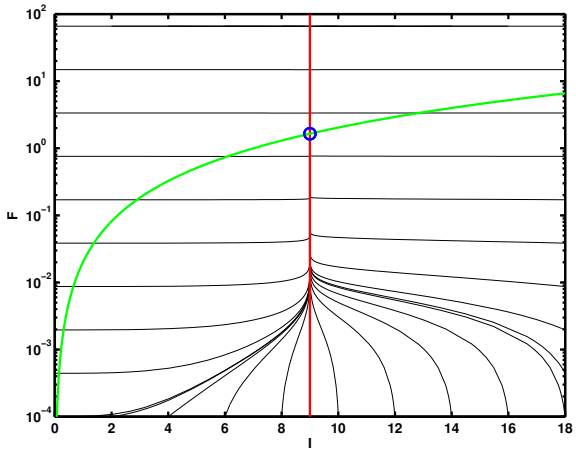

Fig. B.8. **Fig. A4.** Phase-plane portrait for (I, F) in Eqs. (6)-(7).

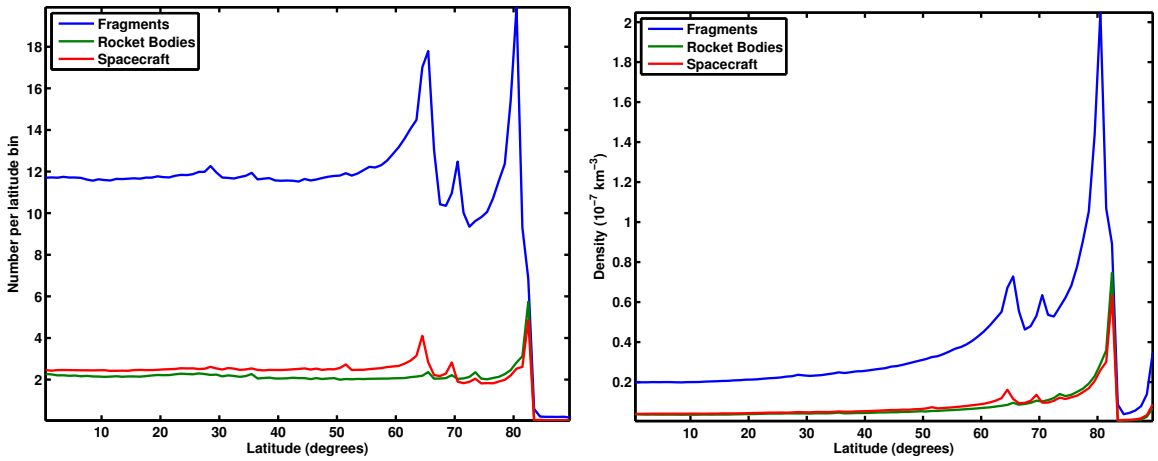

(a) (b)

Fig. B.9. **Fig. B1.** The **(a)** number and **(b)** density of satellites per latitude bin.

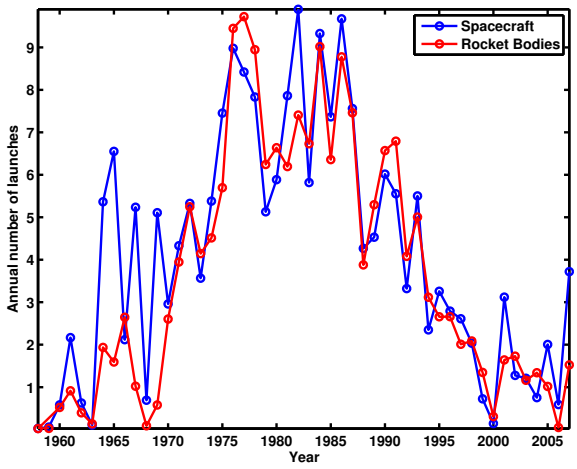

Fig. B.10. **Fig. B2.** Effective number of spacecraft and rocket bodies inserted into the SOI by year.

Table B.1
Parameter values for Eqs. (1)-(5).

$\tilde{\beta}$	R	S	F_R^h	F_R^b	F_S^h	F_S^b
R	2.55×10^{-7}	1.36×10^{-7}	7.64×10^{-8}	6.70×10^{-8}	7.18×10^{-8}	6.68×10^{-8}
S		5.42×10^{-8}	2.02×10^{-8}	1.51×10^{-8}	1.77×10^{-8}	1.50×10^{-8}
F_R^h			3.67×10^{-9}	1.17×10^{-9}	2.58×10^{-9}	1.26×10^{-9}
F_R^b				1.86×10^{-10}	6.30×10^{-10}	1.75×10^{-10}
F_S^h					1.66×10^{-9}	6.66×10^{-10}
F_S^b						1.64×10^{-10}

$\frac{\delta^{Rh}}{\beta}$	R	S	F_R^h	F_R^b	F_S^h	F_S^b
R	75.57	37.78	43.76	0	44.79	0
S		0	-1.00	0	0	0
F_R^h			0	0	0	0
F_R^b				0	0	0
F_S^h					0	0
F_S^b						0

$\frac{\delta^{Rb}}{\beta}$	R	S	F_R^h	F_R^b	F_S^h	F_S^b
R	279.73	139.87	165.68	-1.00	165.80	0
S		0	0	-1.00	0	0
F_R^h			0	0	0	0
F_R^b				0	0	0
F_S^h					0	0
F_S^b						0

$\frac{\delta^{Sh}}{\beta}$	R	S	F_R^h	F_R^b	F_S^h	F_S^b
R	0	98.19	0	0	-1.00	0
S		196.38	115.99	0	115.21	0
F_R^h			0	0	0	0
F_R^b				0	0	0
F_S^h					0	0
F_S^b						0

$\frac{\delta^{Sb}}{\beta}$	R	S	F_R^h	F_R^b	F_S^h	F_S^b
R	0	165.64	0	0	0	-1.00
S		331.29	195.66	0	196.04	-1.00
F_R^h			0	0	0	0
F_R^b				0	0	0
F_S^h					0	0
F_S^b						0

Table B.2
Parameter values for the fragment-fragment version of Eqs. (1)-(5).

$\tilde{\beta}$	R	S	F_R^h	F_R^b	F_S^h	F_S^b
R	2.55×10^{-7}	1.36×10^{-7}	7.64×10^{-8}	6.70×10^{-8}	7.18×10^{-8}	6.68×10^{-8}
S		5.42×10^{-8}	2.02×10^{-8}	1.51×10^{-8}	1.77×10^{-8}	1.50×10^{-8}
F_R^h			3.64×10^{-9}	1.17×10^{-9}	2.59×10^{-9}	1.26×10^{-9}
F_R^b				1.86×10^{-10}	6.29×10^{-10}	1.75×10^{-10}
F_S^h					1.66×10^{-9}	6.67×10^{-10}
F_S^b						1.64×10^{-10}

$\frac{\delta^{Rh}}{\beta}$	R	S	F_R^h	F_R^b	F_S^h	F_S^b
R	75.57	37.78	44.54	0	44.79	0
S		0	0.36	0	0	0
F_R^h			7.98	3.59	5.30	4.39
F_R^b				0	0	0
F_S^h					0	0
F_S^b						0

$\frac{\delta^{Rb}}{\beta}$	R	S	F_R^h	F_R^b	F_S^h	F_S^b
R	279.73	139.87	168.57	-0.79	165.80	0
S		0	5.03	-0.78	0	0
F_R^h			36.93	16.77	23.32	19.94
F_R^b				1.85	-0.07	1.03
F_S^h					0	0
F_S^b						0

$\frac{\delta^{Sh}}{\beta}$	R	S	F_R^h	F_R^b	F_S^h	F_S^b
R	0	98.19	0	0	0.62	0
S		196.38	115.99	0	117.67	0
F_R^h			0	0	8.24	0
F_R^b				0	9.59	0
F_S^h					22.62	11.53
F_S^b						0

$\frac{\delta^{Sb}}{\beta}$	R	S	F_R^h	F_R^b	F_S^h	F_S^b
R	0	165.64	0	0	2.73	-0.71
S		331.29	195.66	0	200.19	-0.70
F_R^h			0	0	15.58	-0.04
F_R^b				0	17.87	1.35
F_S^h					41.53	21.27
F_S^b						2.94

Table B.3
The nonuniformity parameters $f_{\alpha\gamma}$ derived in §B.2.3.

f	F	R	S
F	1.38	1.39	1.33
R		1.72	1.55
S			1.44

Table B.4
The inverse of the decay rates (in years) derived in §B.4.

μ^{-1}	R	S	F_R^h	F_R^b	F_S^h	F_S^b
	1.10×10^4	1.10×10^4	1.23×10^3	3.12×10^2	2.64×10^3	7.57×10^2